crystals

MDPI

Review

Bulk and Single Crystal Growth Progress of Iron-Based Superconductors (FBS): 1111 and 1144

Shiv J. Singh [1,*] and Mihai I. Sturza [2]

[1] Institute of High Pressure Physics, Polish Academy of Sciences, ul. Sokolowska, 29/37, 01-142 Warsaw, Poland
[2] Leibniz Institute for Solid State and Materials Research, IFW Dresden, Helmholtzstr, 20, 01069 Dresden, Germany; m.i.sturza@ifw-dresden.de
* Correspondence: sjs@unipress.waw.pl; Tel.: +48-22-632-50-10

Abstract: The discovery of iron-based superconductors (FBS) and their superconducting properties has generated huge research interest and provided a very rich physics high T_c family for fundamental and experimental studies. The 1111 (*RE*FeAsO, *RE* = Rare earth) and 1144 ($AEAFe_4As_4$, *AE* = Ca, Eu; *A* = K, Rb) families are the two most important families of FBS, which offer the high T_c of 58 K and 36 K with doping and without doping, respectively. Furthermore, the crystal growth of these families is not an easy process, and a lot of efforts have been reported in this direction. However, the preparation of high-quality and suitable-sized samples is still challenging. In this short review, we will summarize the growth of materials with their superconducting properties, especially polycrystals and single crystals, for the 1111 and 1144 families, and make a short comparison between them to understand the developmental issues.

Keywords: high T_c superconductors; transition temperature; synthesis and crystal growth; polycrystalline and single crystal; iron-based superconductors

Citation: Singh, S.J.; Sturza, M.I. Bulk and Single Crystal Growth Progress of Iron-Based Superconductors (FBS): 1111 and 1144. *Crystals* **2022**, *12*, 20. https://doi.org/10.3390/cryst12010020

Academic Editor: Andrei Vladimirovich Shevelkov

Received: 11 November 2021
Accepted: 17 December 2021
Published: 23 December 2021

1. Introduction

In 1911, superconductivity was first discovered in mercury metal by electrical conductivity measurement [1]. Subsequently, many compounds have been exposed as superconductors with an increasing high transition temperature (T_c) during some intervals of time [2]. However, the real mechanism of this fascinating quantum phenomenon is still not understood [2]. The new iron-based superconductor (FBS) has generated enormous interest in this direction, and many research activities are currently going on with various kinds of FBS [3–5]. FBS was discovered in 2008 through F doped LaFeAsO, which crystallizes with a tetragonal layered ZrCuSiAs structure, and after that, many compounds have been discovered [6], most of which display superconductivity through suitable doping. FBS became the second high-T_c-superconducting family after cuprate superconductors and has been the subject of extensive research into their physical nature and application potential [3,4,7,8]. On the basis of the crystal structures of the parent compounds [3,7], FBS can be categorized into several families and abbreviated as: 1111 (*RE*FeAsO, *RE* = Rare earth) [6], 122 as $AeFe_2As_2$ (*Ae* = Ca, Sr, Ba), or AFe_2As_2 (*A* = K, Rb, Cs) or $REFe_2As_2$ (*RE* = Eu) [5,7,9,10], 11 representing Fe*X* (*X* = chalcogenide) [5], 111 being *A*FeAs (*A* = Li, Na) [5,11] and 1144 ($AEAFe_4As_4$, *AE* = Ca, Eu; *A* = K, Rb) [12]. Another group of FBS with thick perovskite-type oxide blocking layers includes $Sr_3Sc_2O_5Fe_2As_2$ (32522) [13], $Sr_4Sc_2O_6Fe_2P_2$ (42622) [14], $Sr_4V_2O_6Fe_2As_2$ (42622), $(Ca_4(Mg_{0.25}Ti_{0.75})_3O_8)(Fe_2As_2)$ (43822) [15], and $(Ca_5(Sc_{0.5}Ti_{0.5})_4O_{11}(Fe_2As_2)$ (541122) [16]. More details about the crystal structures of FBS families and their abbreviations are depicted in Figure 1.

FBS has a very high upper critical field (H_{c2}) (above 100 T), a small electromagnetic anisotropy (γ = 1.5–2 for the 122 and 1144 families near their T_c), a relatively high T_c of up to 58 K, and a large critical current density (J_c) of 10^7–10^8 A/cm^2 at low temperatures [3,7,17,18]. The effectiveness of various modes of doping is one of the outstanding

characteristics of FBS, which results in a rich variety of superconducting materials. In particular, the 122, 11, and 1144 families have almost isotropic properties at low temperatures [4,7,8], implying high irreversibility fields H_{irr} close to H_{c2} values and a strong potential comparable to cuprate superconductors [8]. These properties are fairly favorable for the design and operation of high-field magnets. At 4.2 K (liquid He temperature), the H_{c2} values of the 1111, 122, and 1144 families are much higher than that (below 25 T) of MgB_2 superconductor [19] and the conventional superconductors NbTi, Nb_3Sn [8,17]. Interestingly, the high field behavior of FBS may enable the development of cryogen-free instruments such as superconducting magnets that operate at liquid hydrogen temperatures (~20 K) [3,4,8,20].

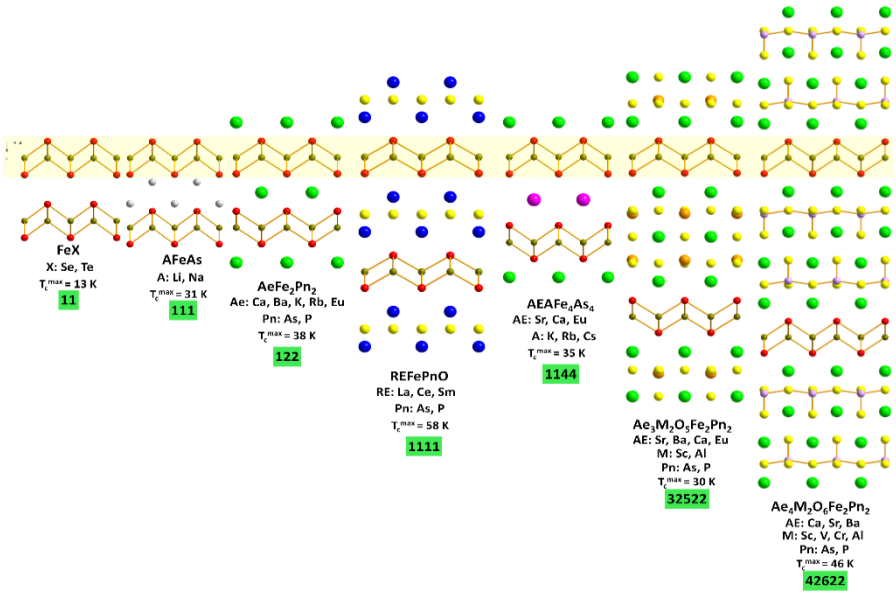

Figure 1. Various crystal structures of Iron-Based Superconductor (FBS) families with details of their abbreviations according to their stoichiometry.

Generally, the parent compound of iron pnictides is usually a bad metal with structural and antiferromagnetic transitions at low temperatures [5]. Superconductivity emerges from an antiferromagnetic spin-density-wave (SDW) phase in most FBS families by applying pressure or changing the electronic structure via iso- or hetero-valent substitution (commonly referred to as electron- or hole-doping) [5]. The SDW transition is usually associated with a structural transition from high-temperature tetragonal to low-temperature orthorhombic symmetry at the same or slightly higher temperature [5]. In summary, three types of long-range order often manifest in the low-temperature phase of FBS: (i) orbital ordering, (ii) orthorhombic distortion, and (iii) the antiferromagnetic SDW order. All of these are intimately linked to each other, and all of them break *C4*-symmetry [21,22]. Before these long-range ordered states, a phase with lower rotational point group symmetry but with time-reversal symmetry being preserved occurs and is referred to as "nematic" [21–24]. Hence, the formation of the nematic phase represents a chicken-egg scenario where it is unclear which phase drives which and how this is linked to the occurrence of superconductivity. Until now, the nematic phase has been widely studied in 122 and 11 families [23,24], while nematicity in the 1111 family is almost unexplored [22]. Addressing this complex state of matter requires single crystals of appropriate size and quality with different types of substitution (iso-and hetero-valent, in-and out-of-plane, non-magnetic, or magnetic elements) and well-defined concentrations.

Most compounds show superconductivity by suitable doping or applied external pressure [5], whereas the 11, 111 and 1144 families are stoichiometric superconductors with T_c of ~8 K, 18 K and 37 K, respectively [7,12,17] at ambient pressure. In the case of the

122 family, the hole-doped $BaFe_2As_2$ such as ((Ba,K)Fe_2As_2) exhibits the highest T_c up to 38 K [10], whereas the electron-doped 122 such as (Ba($Fe_{1-x}Co_x$)$_2As_2$) shows the T_c up to 22 K [9] and the rare earth doped 122 ($Ca_{1-x}RE_xFe_2As_2$ superconductors (*RE* = rare earth elements)) system shows the enhancement of the T_c up to 49 K in $Ca_{1-x}Pr_xFe_2As_2$ [3,5]. In the 111 family, the highest T_c of up to 18 K is observed in LiFeAs, and in the case of NaFeAs, the highest T_c can reach up to 31 K under the applied external pressure (~3 GPa) [25]. The simplest 11 family, i.e., the parent FeSe depicts the T_c of 8 K which has been enhanced up to 37 K under high-pressure studies [26]. This transition temperature has been enhanced up to 40 K by intercalation of alkali metal into the FeSe layer at the ambient pressure and up to 48 K by high-pressure studies in the composition $K_{0.8}Fe_{1.7}Se_2$ [27]. Surprisingly, the highest T_c for the 11 family is reported at up to 100 K in the monolayer FeSe thin films [28]. Aside from these families, many other FBS with lower transition temperatures have been reported, including $Ca_{10}(Pt_3As_8)(Fe_2As_2)_5$, LaFeSiH, $Sr_4Sc_2O_6Fe_2P_2$, Sr_2VO_3FeAs, $Ca_3Al_2O_{5-y}Fe_2Pn_2$ (*Pn* = As and P), and others [5,27]. The highest T_c reported for FBS is around 58 K in fluorine-doped SmFeAsO (Sm1111) [29]. These FBS have unique physics of pairing mechanisms and have a high potential for practical applications due to their high superconducting properties. More than 100 compounds are available under this new FBS, with family 122 ($AeFe_2As_2$, *Ae* = Ba, Sr) having an easier synthesis process to grow high-quality samples than other families, and as a result, this family has received a lot of attention [3,4]. However, it is still challenging to control the exact content of the doping level. For example, the highest superconducting properties have been reported through K-doping, where the control of exact doping content is also a difficult task [3,4,17].

Furthermore, various studies have shown that this new high T_c FBS family has a weak-link effect of high angle grain boundaries similar to high T_c cuprates [11,16,30–33]. Earlier reported FBS samples contained many impurity phases at the grain boundaries or inside grains [31]. However, the quality of FBS samples has been improved with more studies [29,34]. These studies show that the pure phase samples have very weak grain connections and also have many pores, which generally reduce the transport properties [31,32]. In the case of rare-earth barium copper oxide *RE*BCO (*RE* = Sm, Gd, Eu), when the grain boundary angle is larger than 3 to 5 degrees, the intergrain J_c reduces exponentially with an increasing grain boundary (GB) angle [35]. Based on studies for Ba(Fe, Co)$_2As_2$ (122) films, this critical angle has been reported to be up to 9 degrees for the FBS [33,36]. These studies suggest that FBS has lower weak link effects than that of *RE*BCO superconductors, so one can expect high transport J_c for the FBS wires and tapes using the simple and conventional method, rather than the complex coated conductor techniques as used for cuprate superconductors [4]. The above-mentioned properties of FBS make them a strong contender for high magnetic field applications well beyond the capabilities of other superconductors, such as conventional superconductors [3,8,17].

For high magnetic field applications, long length conductors are needed with high values of superconducting parameters, such as irreversibility field (H_{irr}), upper critical field (H_{c2}), transport critical current density (J_c), and engineering current density (J_e), for cable fabrication and coil winding [8]. For this purpose, we need both high-quality and a large amount of powder samples [4]. The transport J_c is estimated by dividing the critical current (I_c) by the cross-section area of the superconducting core in wires and tapes. Connections between grains, the material density, and the pinning strength are the critical factors in determining the critical current behavior of the type II superconductors [3,17]. On the other hand, the grain connectivity is generally suppressed by the presence of voids, an insulating oxide phase, and imperfect connections between grains [16,32,37].

To understand the precise properties of these families, high-quality crystalline samples with a series of doping contents are needed. However, the preparation of high-quality and suitable-sized single crystals is crucial for studying the anisotropic and intrinsic properties, but in some materials, especially those containing many elements, single crystal preparation is very difficult. It may be possible to grow the crystal in a pristine form, but small deviations from the composition may exist with impurity phases and in the form

of small imperfections. These defects will affect the structure, intrinsic bulk transport, and magnetic properties of the crystal. Some of the FBS families, such as 122, 11, and 111, have a very straight-forward single crystal growth process using either a self-flux technique with a flux such as FeAs, KAs, or NaAs [9,38–40] or another metal like Sn as a solvent [41,42]. As a result, the crystals were available just after their first report [10,42–48]. Generally, the self-flux method is a very common method of crystal growth for FBS because this method avoids the incorporation of foreign elements/atoms that can work as dopants [41]. Other state-of-the-art growth approaches, such as growth from the melt using directional solidification (e.g., by the Bridgman technique), are unfavourable due to the incongruent melting behaviour in combination with rather high melting temperatures as for $BaFe_2As_2$ [49]. The method of choice for such incongruently melting materials would be the floating zone technique, but the high volatility of arsenic (As) prohibits the formation of a stable zone (composition) and therefore prevents the growth of FBS using the floating zone technique [49]. In the case of polycrystalline samples solid-state reaction methods are used, which generally show the combined effect of grains. High-quality precursors and the particle size of the initial powder play an important role in preparing highly dense samples with well-connected grains. From a practical point of view, high-quality powder samples are generally used for the fabrication of superconducting tapes and wires, and bulks [4].

Since the 1111 and 1144 families are strong contenders for the practical applications, they also provide an opportunity to understand the superconducting properties of doped and undoped families [4,17,18]. However, the preparation of high-quality and suitable-sized samples is more challenging for these families, and due to it, there are many contradictions with their properties. For example, the reported T_cs are still limited due to difficulties in doping contents, high synthesis temperatures, and vaporization of arsenic and other lighter elements such as fluorine, potassium [5,50]. Furthermore, among the complex vortex phenomena, the second magnetization peak (SMP, also known as the fishtail effect) in the field-dependent magnetization (MHL) measurements is widely observed in various kinds of FBS [18]. In FBS, SMP has been observed in all of the five main families 11 [51], 111 [52], 122 [53], 1144 [18], 1111 [54] (Figure 1). However, similar to cuprates, different explanations are proposed [18,52,54]. In addition, SMP is observed in some crystals but absent in others, and the reasons are still unknown. Reports based on $CaKFe_4As_4$ (1144) show some abnormal vortex dynamics behaviours, such as the huge differences from 10^5 to 10^7 A/cm^2 in J_c along $H//c$, and another exception is that the fishtail effect is observed in some 1144 crystals but absent in others [17,55,56], and the reasons are still unclear. So, the debate on their properties is still open, and no clear understanding has been reached yet. The basic reason for these problems could be the lack of a robust synthesis process and high-quality samples, which are the main motivation for this paper. In this short review, we will mainly focus on the progress of the superconducting properties of the 1111 and 1144 families of FBS concerning their reported single crystal growth and polycrystal synthesis processes.

2. Family 1111

In the FBS families, the 1111-type superconductors have been holding the record for T_c in bulk materials with several reports [29,57,58]. This family is represented by the general formula REFeAs$O_{1-x}F_x$ (RE = La, Ce, Pr, Nd, Sm, Gd, Tb, Dy) [5], which is abbreviated as RE1111 or 1111, as shown in Figure 1. These compounds crystalize in the tetragonal space group *P4/nmm*, with ZrCuSiAs -type structure [6] with insulating layers REO and conducting blocks FeAs. The structure consists of alternating REO and FeAs layers, which are electrically charged and represented as $(RE\text{O})^{+\alpha}(\text{FeAs})^{-\alpha}$. It has been confirmed the strong covalent character in the FeAs layer and the strong ionic character in the REO layer [5]. Electron carriers can be introduced by substituting F for O or by oxygen deficiency. By substituting Sr^{2+} for La^{3+} in La1111, holes are introduced [59].

The 1111-type bulk superconductors have been widely studied to achieve a record T_c by various doping methods, external pressure, or synthesizing techniques [29,57,58].

Following the first report of $LaFeAsO_{1-x}F_x$ with T_c around 26 K [6], a high-pressure synthesis method quickly observed an increase in T_c up to 55 K in $SmFeAsO_{1-x}F_x$ and $SmFeAsO_{1-\delta}$ [60]. Usually, the electron doping in 1111 such as F doping in the LaO layer of La1111 [61], Th doping in the LaO layer of La1111 [62], and even H doping in the LaO layer [3] results in almost similar T_c, whereas the chemical doping in superconducting FeAs layers [63–67] generally leads to a lowering of T_c such as Co, Mn, Ni, P doped FeAs layer [65–67] as mentioned in Table 1. The effects of applied external pressure on the transition temperature have also been studied for this 1111 family [27]. Interestingly, the applied pressure improved the superconducting transition T_c from 26 K to 43 K for $LaFeAsO_{0.89}F_{0.11}$ (La1111), nevertheless, it reduced the T_c for $CeFeAsO_{0.88}F_{0.12}$ (Ce1111) and $REFeAsO_{0.85}$ (RE1111) (*RE* = Sm and Nd) [27]. Moreover, superconductivity at 57.8 K was found in $SmFeAsO_{1-x}F_x$ film grown by molecular beam epitaxy [36]. Recently, several groups found that low-temperature sintering and slow-cooling techniques could introduce high F-doping levels with T_c enhanced up to 58 K in $SmFeAsO_{1-x}F_x$ [29,57]. Furthermore, the Th and F co-doped $Sm_{1-x}Th_xFeAsO_{1-y}F_y$ samples synthesized by the solid-state reaction can effectively enhance superconductivity, resulting in a maximum T_c of 58.6 K [58].

Table 1. A list of polycrystalline samples reported for the 1111 (*RE*FeAsO) and 1144 ($AEAFe_4As_4$) families, along with their synthesis conditions and superconducting properties. T^{syn} is used for the synthesis temperature and heating time. The Solid-State Reaction (SSR) method at high pressure and ambient pressure is represented by the high-pressure synthesis technique (HPST) and the conventional synthesis process at ambient pressure (CSP-AP), respectively.

Sample	Synthesis Method and Conditions	Superconducting Properties
LaFeAs(O,F)	CSP-AP, T^{syn} = 1180 °C, 48 h	T^{max}_c = 28.5 K, $H_{c2}(0)$ = 105 T [61]
(La,K)FeAs(O,F)	CSP-AP, T^{syn} = 1180 °C, 48 h	T^{max}_c = 26.5 K, $H_{c2}(0)$ = 122 T [61]
$LaFeAsO_{1-y}$	HPST, T^{syn} = 1100–1200 °C, 2 h	T^{max}_c = 28 K [68]
(La,Sr)FeAs	CSP-AP, T^{syn} = 1150 °C, 40 h	T^{max}_c = 26 K [59]
(La,Y)FeAs(O,F)	CSP-AP, T^{syn} = 1250 °C, 25 h	T^{max}_c = 40.2 K, $H_{c2}(0)$ = 60.5 T [69,70]
$(La,Y)FeAsO_{0.6}$	HPST, T^{syn} = 1150 °C, 2 h	T^{max}_c = 43.1 K [71]
LaFe(As,Sb)(O,F)	CSP-AP, T^{syn} = 1150 °C, 48 h	T^{max}_c = 30.1 K, $H_{c2}(0)$ = 73 T [72]
La(Fe,Co)AsO	CSP-AP, T^{syn} = 1220 °C, 12 h	T^{max}_c = ~14.3 K [73]
(La,Th)FeAsO	CSP-AP, T^{syn} = 1180 °C, 48 h	T^{max}_c = 30.3 K, $H_{c2}(0)$ = 47 T [62]
LaFe(As,P)O	CSP-AP, T^{syn} = 1100 °C, 40 h	T^{max}_c = 10 K, $H_{c2}(0)$ = 27 T [74]
$LaFe_{0.95}Co_{0.05}AsO_{0.89}F_{0.11}$	CSP-AP, T^{syn} = 1150 °C, 48 h	T^{max}_c = ~15 K [75]
$LaFe_{0.99}Co_{0.01}AsO_{0.89}F_{0.11}$	CSP-AP, T^{syn} = 1150 °C, 48 h	T^{max}_c = ~10 K [75]
$LaFeAsO_{0.6}H_{0.6}$	HPST, T^{syn} = 1100 °C, 2 h	T^{max}_c = ~38.3 K [76]
CeFeAs(O,F)	CSP-AP, T^{syn} = 1180 °C, 48 h	T^{max}_c = 42.5 K, $H_{c2}(0)$ = 94 T [77]
(Ce,Y)FeAs(O,F)	CSP-AP, T^{syn} = 1100 °C, 30 h	T^{max}_c = 48.6 K, $H_{c2}(0)$ = 90 T [78]
CeFe(As,P)O	CSP-AP, T^{syn} = 1175 °C, 50 h	T^{max}_c ~4 K [79,80]
$CeFe(As,P)O_{0.95}F_{0.05}$	CSP-AP, T^{syn} = 1175 °C, 50 h	T^{max}_c = 21.3 K [81]
Ce(Fe,Co)As(O,F)	CSP-AP, T^{syn} = 1150 °C, 48 h	T^{max}_c = 23.4 K, $H_{c2}(0)$ = 25.3 T [82]
Ce(Fe,Co)AsO	CSP-AP, T^{syn} = 1180 °C, 48 h	T^{max}_c = 11.31 K, $H_{c2}(0)$ = 45.2 T [64]
Ce(Fe,Ni)AsO	CSP-AP, T^{syn} = 1150 °C, 48 h	No T_c [66]
Ce(Fe,Zn)AsO	CSP-AP, T^{syn} = 1150 °C, 48 h	No T_c [66]
CeFe(As,Sb)(O,F)	CSP-AP, T^{syn} = 1180 °C, 48 h	T^{max}_c = 43.17 K, $H_{c2}(0)$ = 137 T [83]
$CeFeAsO_{0.6}H_{0.6}$	HPST, T^{syn} = 1100 °C, 2 h	T^{max}_c = ~47.9 K [76]
PrFeAs(O,F)	CSP-AP, T^{syn} = 1150 °C, 24 h	T^{max}_c = 50 K [84]
Pr(Fe,Co)AsO	CSP-AP, T^{syn} = 1100 °C, 48 h	T^{max}_c = 16 K, $H_{c2}(0)$ = 50.2 T [63]
(Pr,Sr)(Fe,Co)AsO	CSP-AP, T^{syn} = 1160 °C, 40 h	T^{max}_c = 16 K [85]
$PrFeAsO_{0.6}H_{0.6}$	HPST, T^{syn} = 1100 °C, 2 h	T^{max}_c = ~51.9 K [76]
$NdFeAsO_{1-y}$	HPST, T^{syn} = 1100–1200 °C, 2 h	T^{max}_c = 54 K [68,86]
NdFeAs(O,F)	CSP-AP, T^{syn} = 1350 °C, 15 h	T^{max}_c = 55 K [87,88]
(Nd,Gd)FeAs(O,F)	CSP-AP, T^{syn} = 1350 °C, 15 h	T^{max}_c = 55.1 K, J_c(5K) = 3.4 × 10^3 A/cm^2 [89]
Nd(Fe,Rh)AsO	CSP-AP, T^{syn} = 1150 °C, 48 h	T^{max}_c = 18 K, $H_{c2}(0)$ = 100 T [90]
$NdFe_{0.85}Ru_{0.15}AsO_{0.89}F_{0.11}$	CSP-AP, T^{syn} = 1150 °C, 48 h	T^{max}_c = 34 K [91]
$NdFe_{0.9}Co_{0.1}AsO_{0.89}F_{0.11}$	CSP-AP, T^{syn} = 1150 °C, 48 h	T^{max}_c = ~18 K [75]
$NdFe_{0.98}Mn_{0.02}AsO_{0.89}F_{0.11}$	CSP-AP, T^{syn} = 1150 °C, 48 h	T^{max}_c = ~27 K [75]
$Nd_{0.99}Ca_{0.01}FeAsO_{0.8}F_{0.2}$	CSP-AP, T^{syn} = 1150 °C, 20 h	T^{max}_c = ~48 K [92]

Table 1. *Cont.*

Sample	Synthesis Method and Conditions	Superconducting Properties
Nd(Fe,Co)AsO	CSP-AP, T^{syn} = 1150 °C, 48 h	T^{max}_c = ~16.5 K, $H_{c2}(0)$ = 26 T [93]
SmFeAs(O,F)	CSP-AP, T^{syn} = 900 °C, 45 h	T^{max}_c = 57.8 K, $H_{c2}(0)$ = 315 T [29]
SmFeAs(O,F)	CSP-AP, T^{syn} = 980 °C, 40 h	T^{max}_c = 58.1 K [57]
(Sm,Th)FeAs(O,F)	CSP-AP, T^{syn} = 1150 °C, 30 h	T^{max}_c = 58.6 K [58]
Sm(Fe,Co)AsO	CSP-AP, T^{syn} = 1180 °C, 45 h	T^{max}_c = 15.2 K [94]
(Sm,Sc)FeAs(O,F)	CSP-AP, T^{syn} = 950 °C, 2 h	T^{max}_c = 53.5 K, $H_{c2}(0)$ = 298 T [95]
(Sm,Th)FeAsO	CSP-AP, T^{syn} = 1150 °C, 30 h	T^{max}_c = 45 K [58]
$Sm_{0.9}Y_{0.1}FeAsO_{0.8}F_{0.2}$	CSP-AP, T^{syn} = 1300 °C, 40 h	T^{max}_c = 43 K [96]
Sm(Fe,Ir)AsO	CSP-AP, T^{syn} = 1150 °C, 48 h	T^{max}_c = 16 K [97]
$SmFe_{0.97}Mn_{0.03}As(O,F)$	CSP-AP, T^{syn} = 900 °C, 45 h	T^{max}_c = 30 K, $H_{c2}(0)$ = 205 T [65]
$SmFe_{0.94}Mn_{0.06}AsO_{0.88}F_{0.12}$	CSP-AP, T^{syn} = 900 °C, 45 h	T^{max}_c = 16.5 K, $H_{c2}(0)$ = 43 T [65]
$SmFe_{0.94}Ni_{0.06}AsO_{0.88}F_{0.12}$	CSP-AP, T^{syn} = 900 °C, 45 h	T^{max}_c = 18 K, $H_{c2}(0)$ = 47 T [65]
$SmFe_{0.94}Ni_{0.03}AsO_{0.88}F_{0.12}$	CSP-AP, T^{syn} = 900 °C, 45 h	T^{max}_c = 33 K, $H_{c2}(0)$ = 200 T [65]
$SmFeAs_{0.95}P_{0.05}O_{0.88}F_{0.12}$	CSP-AP, T^{syn} = 900 °C, 45 h	T^{max}_c = 40 K, $H_{c2}(0)$ = 292 T [67]
$SmFeAs_{0.8}P_{0.2}O_{0.88}F_{0.12}$	CSP-AP, T^{syn} = 900 °C, 45 h	T^{max}_c = 20 K, $H_{c2}(0)$ = 31 T [67]
$SmFeAsO_{1-x}$	HPST, T^{syn} = 1300 °C, 2 h	T^{max}_c = 57 K, $H_{c2}(0)$ = 60 T [60]
(Gd,Th)FeAsO	HPST, T^{syn} = 1300 °C, 2 h	T^{max}_c = 56 K [98]
$GdFeAsO_{1-x}$	HPST, T^{syn} = 1350 °C, 2 h	T^{max}_c = 56 K [99,100]
GdFeAs(O,F)	HPST, T^{syn} = 1350 °C, 2 h	T^{max}_c = 51.2 K, $H_{c2}(0)$ = 20 T [99]
GdFeAs(O,F)	CSP-AP, T^{syn} = 1150 °C, 48 h	T^{max}_c = 36.6 K [101]
Gd(Fe,Ir)FeAsO	CSP-AP, T^{syn} = 1200 °C, 72 h	T^{max}_c = 18.9 K, $H_{c2}(0)$ = 24 T [102]
$Sr_{1-x}Sm_xFeAsF$	CSP-AP, T^{syn} = 1000 °C, 10 h	T^{max}_c = 56 K [103]
$CaFe_{1-x}Co_xAsF$	CSP-AP, T^{syn} = 1000 °C, 10 h	T^{max}_c = 22 K [104]
$CaKFe_4As_4$	CSP-AP, T^{syn} = 860–920 °C, 2–6 h	T^{max}_c = 33.1 K [12]
$CaRbFe_4As_4$	CSP-AP, T^{syn} = 860–920 °C, 2–6 h	T^{max}_c = 35 K [12]
$CaCsFe_4As_4$	CSP-AP, T^{syn} = 860–920 °C, 2–6 h	T^{max}_c = 31.6 K [12]
$SrRbFe_4As_4$	CSP-AP, T^{syn} = 860–920 °C, 2–6 h	T^{max}_c = 35.1 K [12]
$SrCsFe_4As_4$	CSP-AP, T^{syn} = 860–920 °C, 2–6 h	T^{max}_c = 36.8 K [12]
$CaKFe_4As_4$	CSP-AP, T^{syn} = 955 °C, 6 h	T^{max}_c = 34.2 K, $H_{c2}(0)$ = 138 T [32]

Polycrystalline samples: These samples are prepared by Solid-State Reaction methods (SSR) which generally provide an important processing route through solid-state diffusion to get a thermodynamically stable phase at high-temperature sintering. Many reports are based on the study of polycrystalline samples prepared by the SSR method as mentioned in Table 1, where SSR at ambient pressure and high pressure is referred to as "Conventional Synthesis Process at ambient pressure (CSP-AP)" and "High-pressure synthesis techniques (HPST)", respectively. Due to the air sensitivity of the precursors, the initial process of the synthesis was performed inside the glove box and sealed into the evacuated quartz tube containing an internal inert crucible or a metal tube, as shown in Figure 2. The 1111 family is very versatile concerning various kinds of doping, such as F doping at O-sites, Co/Ni/Mn/Zn doping at Fe-sites, and Sb/P doping at As sites in parent *RE*FeAsO compounds (Table 1). Generally, the highest T_c is obtained by F doping, and a lot of work has been done with F-doping, but the control of this dopant according to the composition is not a very easy task through CSP-AP. In contrast, since the 1111-type compounds contain at least four components, in the case of dopants, more than five elements are included, and precisely controlling their composition is very difficult. During the initial synthesis process, even if starting materials are mixed at the correct composition ratio, the prepared substance contains a spurious phase whose composition differs from the nominal one for many polycrystalline materials. For example, in the case of Sm1111, the impurity phases of SmOF, SmAs, and/or Sm_2O_3 are formed, and their concentrations generally increase as the dopant concentration increases in $SmFeAsO_{1-x}F_x$ [29,34]. It is a very common situation for other members of the 1111 family, especially those containing rare earth elements. The impurity phase of *RE*FO is stable, and it is not so easy to eliminate. From quantitative analysis, Malavasi et al. [105] demonstrated the difference in composition between nominal and prepared $NdFeAsO_{12x}F_x$ and noted that the measured F-content in a specimen with the nominal composition of $NdFeAsO_{0.78}F_{0.22}$ is 0.188. The relationship between the nominal F content and the real one is determined through electron probe microanalysis [105].

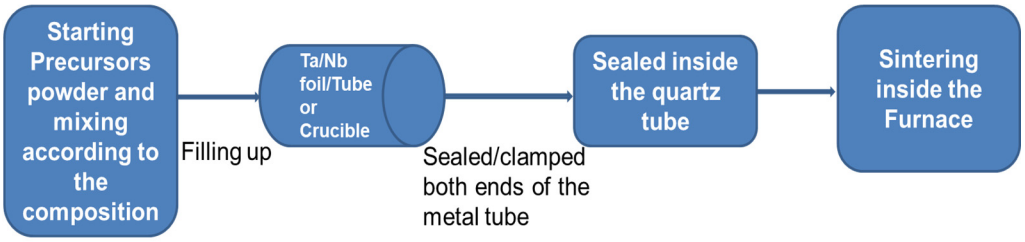

Figure 2. A general block diagram of the Solid-State Reaction (SSR) method for FBS.

To overcome these problems, a high-pressure solid-state reaction method has been used for the 1111 family. The high-pressure synthesis technique (HPST) has been utilized for preparing a series of oxygen-deficient *RE*FeAsO (*RE* = La and Nd) polycrystalline samples [68,86]. The introduction of oxygen vacancies causes a decrease in lattice parameters, and superconductivity appears when the *a*- and *c*-axis lattice parameters shrink by 0.1% when compared to undoped compounds (*RE*FeAsO). When *RE* = La is replaced with *RE* = Nd in *RE*1111, the *a*-lattice parameter is decreased by 0.2%, and the maximum T_c is increased from 28 K to 54 K [68,86]. Further O-deficiency in La1111 eventually results in the reduction of T_c [68]. On the other hand, in the case of Nd1111, the maximum T_c value is robust against the introduction of O-deficiency, suggesting that the superconducting region is much narrower for La1111 than for Nd1111 [68,86]. Similarly, hydrogen doping of Sm1111 and Ce1111 is not possible via CSP-AP, but HPST (2 GPa and 1200 °C) can produce a series of H-doped 1111 [3,68]. These studies have depicted the unique behavior of two superconducting domes in the phase diagram and highlight the new findings of FBS that generate the new physics and new doping effects in 1111 by HPST, whereas single dome behavior is observed in the phase diagram of F-doped 1111 through CSP-AP. In the case of H-doped 1111, the first dome is similar to F-doped La1111 (through CSP-AP), but the range of the second dome is much wider than that reported in the F-substituted case for the other rare earth (*RE*) systems [3]. Kametani et al. [31] have reported polycrystalline $SmFeAsO_{0.85}$ and $NdFeAsO_{0.94}F_{0.06}$ bulk samples synthesized by solid-state reaction under high pressure. These samples are better than the CSP-AP samples, but impurity phases and cracks were found during the microstructural analysis. Furthermore, two distinct scales of current, i.e., intergrain and intragrain current, are observed in the reported polycrystalline samples, which suggests an electromagnetic granular nature of 1111 [30,32,37]. It implies that a locally circulating intragrain supercurrent and others due to intergrain pinning exist in the bulk sample. Microstructural analysis shows the presence of macroscopic inhomogeneity, and cracks and wetting amorphous phases at grain boundaries [31]. Because of these extrinsic factors, the intergrain J_c has a very low value for these samples [30,32,37]. Figure 3 summarizes the 1111 family's transition temperature T_c dependence on the reported intergrain J_c with various FBS. Many groups have optimized the synthesis parameters during solid-state reaction methods such as low-temperature synthesis and have improved the sample quality [29,57]. However, the obtained samples always have problems with grain connectivity and impurity phases. For these reasons, the obtained intergrain J_c value of the 1111 family is very small, as shown in Figure 3, for the requirements of practical applications. To improve the grain connectivity and critical current properties, various techniques such as metal additions (Sn, Pb, Ag, Zn, In), cold or hot pressing, and hot isostatic pressing could be useful during the synthesis process of the polycrystalline samples, which generally improve the microstructure as reported for FBS wires/tapes fabrication [4]. For example, Singh et al. have studied the effect of Sn addition in Sm1111, where Sn additions reduced the impurity phases in $SmFeAsO_{0.8}F_{0.2}$ [4,106], increasing clean and well-connected grain boundaries. Remanent magnetization measurements revealed that Sn addition improved the intergrain J_c at 5 K from 1×10^2 to 1.1×10^4 A cm^{-2} for $SmFeAsO_{0.8}F_{0.2}$ and from 4×10^3 to 9.7×10^3 A cm^{-2} for $SmFeAsO_{0.88}F_{0.12}$ [106], as shown in Figure 3. This enhancement of the intergrain J_c might be attributable to the strong intergrain coupling due to the improved grain connectivity by the Sn additions. However, these obtained values

are still much lower than the practical level, which suggests further improvement of grain size and grain connections is required by reducing the extrinsic factors [4,31,37,106]. Hence, we need more research in this direction through advanced techniques.

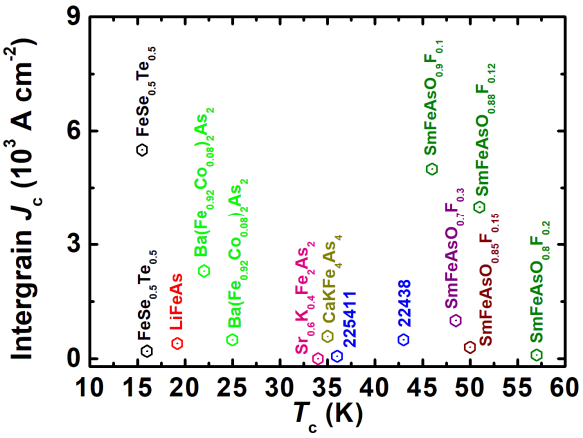

Figure 3. The transition temperature (T_c) dependence of the intergrain J_c calculated from the remanent magnetization measurements for different FBS families together with that of the 1111 and 1144 families. All the mentioned samples are prepared by the conventional synthesis process at ambient pressure (CSP-AP). The data were gathered from the references [11,16,30,32,37,107–110].

Single crystals: Many groups have reported the single crystal growth of this family [50,111–118] using different growth parameters. However, it is not an easy task to obtain high-quality and suitable-sized 1111 crystals. Despite many efforts in the last 12 years, the grown crystals of 1111 are still limited in dimensions [50,118], struggling to keep the nominal composition as the actual composition and to reduce secondary phases or impurities. Due to these problems, the existing results are debatable, and at the moment, a consensus has not been reached yet, similar to other FBS families. For example, a lot of studies have been done on 122 materials with various doping elements (K for Ba, Co for Fe, and P for As) and with different doping concentrations [9,10,119,120]. The reported J_c values determined by magnetic hysteresis loop (MHL) measurements are controversial even for the same types of doped crystals. For example, the doping dependence of J_c follows the doping dependence of T_c for Ba(Fe, Co)$_2$As$_2$, whereas other reports show that J_c does not follow T_c and is highest in the underdoped region for Ba(Fe, Co)$_2$As$_2$ and (Ba, K)Fe$_2$As$_2$ where different pinning sources are also proposed [53,119,121,122]. Extrinsic factors, rather than doping concentration, determine J_c in BaFe$_2$(As,P)$_2$ [119,120]. Due to these issues, there are many unresolved features concerning their superconducting properties. Mostly, the following two methods are used to grow the single crystals of the 1111 family:

(a) Flux methods: Generally, the melt-solidification process cannot work for these compounds due to the presence of many elements that tend to form incongruent melting compounds. Thus, the solution-growth process is needed, and the final growth temperature must be lower than the decomposition temperature of the final compound. In this direction, one of the useful methods is the "flux method". The flux growth method at ambient pressure is used significantly for this family because this method generally helps to start the reaction much lower than that used for solid-state reaction methods. A general block diagram for the self-flux method is shown in Figure 4. The details of the reported 1111 crystals are mentioned in Table 2 with their growth conditions and superconducting properties. FM-AP is used for the Flux method at ambient pressure. Quebe et al. [111] have reported the crystal growth of the parent compound *RE*FeAsO through NaCl/KCl flux. Single crystals of PrFeAsO and NdFeAsO with a size of 70–100 μm have been grown from alkali-metal chloride flux. Fang et al. [113] have used this method to grow NdFeAs and NdFeAsO$_{0.7}$F$_{0.3}$ at ambient pressure. Jesche et al. [114] have grown larger single crystals of CeFeAsO using a Sn-flux technique. Yan et al. [123] used NaAs to grow large single crystals of LaFeAsO,

LaFeAs(O, F), and $LaFe_{0.92}Co_{0.08}AsO$ at ambient pressure, and Jesche et al. [114] used Sn as a flux to grow CeFeAsO at ambient pressure. Nitsche et al. [115] have grown the single crystals of *RE*FeAsO (*RE* = La, Ce, Pr, Nd, Sm, Gd, and Tb) using NaI/KI as flux and obtained crystals with a size of up to 300 µm. The first attempts to grow single crystals following previous studies on $RETM_xAs_2$ (*TM* = transition metal) [116] were conducted with rare-earth metal oxide (RE_2O_3), arsenic, and iron as starting materials, and alkali-metal chlorides as flux. As observed before [50], *RE*OCl hindered the formation of phase-pure samples and single crystals of the target compounds. When using sodium or potassium iodide, the less stable oxide iodides (*RE*OI) are not formed. As an oxygen source, the exchange of rare-earth metal oxide by iron (III)-oxide or better by iron (II)-oxide improved single-crystal growth. However, the synthesis of *RE*FeAsO with rare-earth metals heavier than terbium failed to apply the NaI/KI flux method [111,115]. Unfortunately, according to published papers [20,50], 1111 single crystals via flux growth are difficult to obtain [111,115]. This is because these are oxides facing the hurdle of the low solubility of oxygen in liquid metals at 1100 °C excluding their growth from "classical" metal fluxes and their self-flux variants [124]. However, the ambient pressure reaction process usually limits the synthesis temperature [124–129] and takes a very long time to grow even a tiny crystal size. This process creates chemical inhomogeneity due to the presence of lighter elements and the high vapor pressure of arsenic.

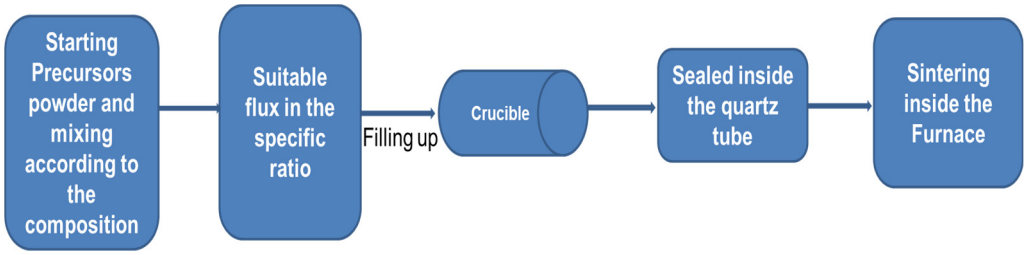

Figure 4. A general block diagram of the flux method.

Table 2. List of single crystals reported for the 1111 (*RE*FeAsO) and 1144 ($AEAFe_4As_4$) families, including growth conditions and superconducting properties. T^{syn} is used for the synthesis temperature and heating time. FM-AP and FM-HP represent Flux method at ambient pressure and the Flux method at high pressure, respectively. SSCG-AP and SSCG-HP refer to the Solid-State Crystal Growth method at ambient pressure and high pressure, respectively.

Sample	Synthesis Method and Conditions	Superconducting Properties
SmFeAs(O,F)	FM-HP, Flux: NCl/KCl, T^{syn} = 1350–1450 °C, 4–85 h	T^{max}_c = 53 K, $H_{c2}(0)$ = ~100 T, J_c(15 K,7 T) = 2 × 10^5 A/cm^2 [50]
REFeAsO	FM-AP, Flux: NaCl/KCl, T^{syn} = 800 °C, 2 weeks	No T_c [111]
$NdFeAsO_{0.9}F_{0.1}$	SSCG-HP, No Flux, T^{syn} = 1350–1400 °C, 8 h	T^{max}_c = 45 K [54,112]
$LaFeAsO_{0.9}F_{0.1}$	SSCG-HP, No Flux, T^{syn} = 1350–1400 °C, 8 h	T^{max}_c = 14 K [112]
$NdFeAsO_{0.7}F_{0.3}$	FM-AP, Flux: NCl, T^{syn} = 1050 °C, 2 weeks	T^{max}_c = 49 K, $H_{c2}(0)$ = 49 T [113]
CeFeAsO	FM-AP, Flux: Sn, T^{syn} = 1500 °C, 1 h	No T_c [114]
$CeFeAs_{0.7}P_{0.3}O$	FM-AP, Flux: Sn, T^{syn} = 1500 °C, 1 h	No T_c [114,129]
SmFeAs(O,F)	FM-AP, Flux: CsCl, T^{syn} = 950 °C, 5 h	T^{max}_c = 57.5 K, $H_{c2}(0)$ = ~330 T [34]
$PrFeAsO_{1-y}$	FM-HP, No Flux/Flux:As/FeAs/PrFeAs(O,F), T^{syn} = 1300–1400 °C, 2 h	T^{max}_c = 44 K [125]
*RE*FeAsO	FM-AP, Flux: NaI/KI, T^{syn} = 1050 °C, 6–7 days	No T_c [115]
$LaFeAsO_{0.91}F_{0.09}$	FM-AP, Flux: NaAs, T^{syn} = 1150 °C, 24 h	T_c = 11 K [123]
$LaFe_{0.98}Co_{0.02}AsO$	FM-AP, Flux: NaAs, T^{syn} = 1150 °C, 24 h	T_c = ~8 K [123]
(La/Nd)FeAsO	FM-AP, Flux: NaAs, T^{syn} = 1100 °C, 12 h	No T_c [126]
LaFeAsO	SSCG-AP, T^{syn} = 1080 °C, 200 h	No T_c [127]

Table 2. *Cont.*

Sample	Synthesis Method and Conditions	Superconducting Properties
$CaFe_{0.882}Co_{0.118}AsF$	FM-AP, Flux: CaAs, T^{syn} = 1230 °C, 20 h	T_c = 22 K [126]
Sm(Fe,Co)AsO	FM-HP, Flux: NaAs/KAs, T^{syn} = 1350–1450 °C, 4–85 h	T_c = 16.4 K, $H_{c2}(0)$ = 100 T, J_c(2K,0T) = 1 × 10^5 A/cm^2 [118]
PrFeAs(O,F)	FM-HP, Flux: NaAs/KAs, T^{syn} = 1350–1450 °C, 4–85 h	T_c = 30 K, J_c(5K,0T) = 1 × 10^5 A/cm^2 [118]
$PrFeAsO_{0.80-x}F_x$	FM-HP, Flux: NaCl/KCl, T^{syn} = 1350–1450 °C, 4–85 h	T_c = 38.3 K [50]
$NdFeAsO_{0.89-x}F_x$	FM-HP, Flux: NaCl/KCl, T^{syn} = 1350–1450 °C, 4–85 h	T_c = 46.3 K [50]
$GdFeAsO_{0.76-x}F_x$	FM-HP, Flux: NaCl/KCl, T^{syn} = 1350–1450 °C, 4–85 h	T_c = 22.7 K [50]
NdFeAs(O,F)	FM-HP, Flux: NaAs/KAs, T^{syn} = 1350–1450 °C, 4–85 h	T_c = 38.5 K [118]
SmFeAs(O,H)	FM-HP, Flux: Na_3As/3NaH+As/Na_3As+3NaH+As, T^{syn} = 1200 °C, 4–85 h	T_c = 43.0 K [20]
$CaKFe_4As_4$	FM-AP, Flux: FeAs, T^{syn} = 1180 °C, 5 h	T_c = 35.0 K, $H_{c2}(0)$ = ~100 T, J_c(2K,0T) = ~10^7–10^8 A/cm^2 [18,130]
$CaK(Fe_{1-x}Ni_x)_4As_4$	FM-AP, Flux: FeAs, T^{syn} = 1180 °C, 5 h	T_c = 9–30 K [131]
$CaK(Fe_{1-x}Co_x)_4As_4$	FM-AP, Flux: FeAs, T^{syn} = 1180 °C, 5 h	T_c = 2–29 K [131]
$CaRbFe_4As_4$	FM-AP, Flux: FeAs, T^{syn} = 1180 °C, 2 h	T_c = 35 K [132]
$EuRbFe_4As_4$	FM-AP, Flux: FeAs, T^{syn} = 1250 °C, 24 h	T_c = 35 K, $H_{c2}(0)$ = ~135 T [133]
$EuRbFe_4As_4$	FM-AP, Flux: RbAs, T_{syn} = 920 °C, 12 h	T_c = 37 K [134,135]

A few groups have tried the high-pressure growth methods [50,54,68,125], which usually enhance the reaction rate and have many advantages over conventional methods. FM-HP is used for the Flux method at high pressure. This high-pressure method enables the high-temperature reaction by reducing the vaporization of lighter elements and also reducing the inhomogeneity of the samples, which speeds up the reaction process. There are only a few reports of 1111 crystal growth by using high-pressure techniques (FM-HP), as mentioned in Table 2, which have resulted in the growth of slightly large and homogeneous crystals. Ishikado et al. [125] have reported the single crystal growth of $PrFeAsO_{1-y}$ in BN crucibles under a pressure of about 2 GPa at 1300–1400 °C for 2 h, and the obtained crystals were around 500 µm. Karpensiki et al. [50] adopted the high-pressure crystal-growth method and produced the *RE*1111 crystals with a size of 300 µm. They carried out a systematic investigation of the parameters controlling the growth of *RE*1111 crystals, including the thermodynamic variables, reagent composition, and kinetic factors such as reaction time and cooling rate. The high-pressure flux method using Na-As and KAs as a flux provided the slightly larger-sized 1111 crystals (up to ~1 mm) which were separated from the flux before its characterization [50]. In comparison with NaCl/KCl flux growth, these fluxes are at least three times more efficient in obtaining large-sized crystals [50]. There are reports that NaAs works as a flux, enabling the uptake of oxygen via the intermediate formation of $NaAsO_2$ yielding small crystals, and sometimes intergrowth with a 122 phase has also been reported [123,124,136]. By applying pressure, SmFeAsO single crystals of up to 150 µm have been obtained. Using high pressure and arsenic as flux, Ishikado et al. [125] obtained large single crystals of the parent PrFeAsO. From pellets of NdFeAsO and LaFeAsO synthesized at high pressure, Martin et al. [112] have been able to isolate crystals with a size up to half a millimeter.

Hence, the 1111 family is currently the least investigated and understood among all FBS, mostly due to the lack of appropriate single crystals. The reported crystals were very tiny and available only for some compositions (Table 2), but the research community needs a series of better single crystals to understand the intrinsic properties and to complete the superconducting phase diagram of 1111 without the extrinsic effects. However, the 1111-phase formation and chemical composition are more difficult to control during the

growth process. The quality of the crystal can be confirmed by structural and compositional analysis, which are related to superconducting properties. High-pressure techniques (FM-HP), on average, produce sufficiently large crystals when compared to conventional growth methods (FM-AP) [50,118]. Thus, to grow large and homogeneous single crystals, further optimization of the growth conditions is required using the pressure method, including the suitable type of flux.

(b) Solid-State Crystal Growth (SSCG) method: This method utilizes the phenomenon of abnormal grain growth to grow single crystals from a polycrystalline matrix. Recently, Kappenberger et al. [127] reported the growth of large 3-dimensional and facetted single crystals of the parent compound LaFeAsO only using solid-state single crystal growth at ambient pressure (SSCG-AP), as shown in Figure 5. This unconventional crystal growth method was successfully used for the first time to grow LaOFeAs crystals with high quality as well as good physical properties. A schematic representation of the SSCG method for growing 1111 single crystals is presented in Figure 5a.

First, a polycrystalline sample of LaFeAsO was prepared using a two-step solid-state reaction method. Afterward, the polycrystalline powder and Na-As powder in a volume ratio of about 1:1 were layered into an alumina crucible. The Na-As powder melted into a liquid phase at around 550 °C during annealing, diffused into the pores of the polycrystalline compact, and promoted crystal growth. The most important aspect to be mentioned in this report is that NaAs are not a flux, as sometimes misinterpreted in the literature, but only aids in increasing interfacial anisotropy as a trigger for abnormal grain growth [127]. Representative crystals with pronounced facets are shown in Figure 5b. These kinds of three-dimensional and faceted crystals are typical for this SSCG method but very uncommon for crystals of the pnictide superconductors and especially for the oxypnictides [127]. This method has been used to grow the crystal for parent compounds, but F-doped 1111 was not successful [127]. Martin et al. [54,112] have grown single crystals of $LaFeAsO_{0.9}F_{0.1}$ and $NdFeAsO_{0.9}F_{0.1}$ using the Solid-State Crystal Growth method at high pressure (SSCG-HP) without the use of a mediator powder (Table 2). The crystals were extracted from 5 mm diameter pellets synthesized under high pressure and high temperature, and the value of 10% F substitution is nominally based on the initial stoichiometry of the pellet. More work is needed in this direction with various kinds of doping content.

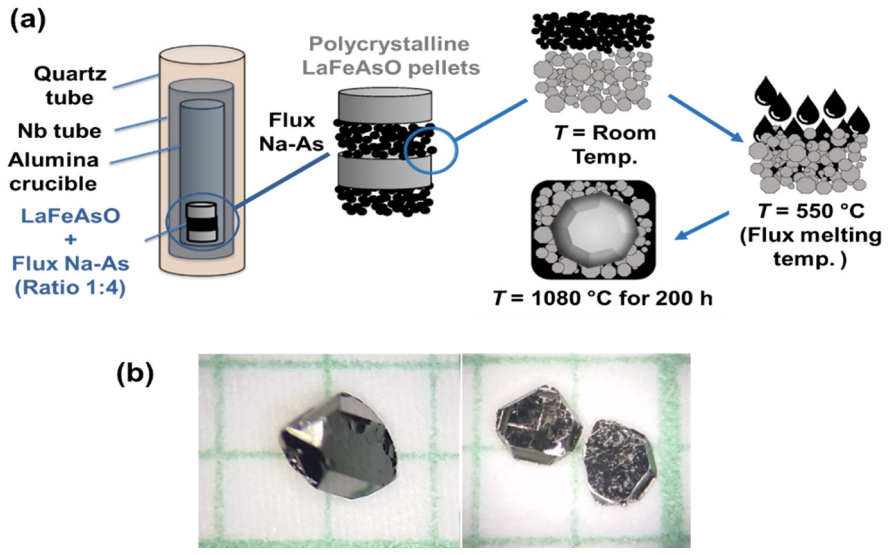

Figure 5. (**a**) A block diagram of the Solid-State Crystal Growth (SSCG) process at ambient pressure (SSCG-AP). The Na-As, as the liquid medium promotor for the growth, is used in between the polycrystalline LaFeAsO pellets. After annealing, a bimodal size distribution has developed, including large, faceted crystals. (**b**) The grown LaFeAsO single crystals with pronounced facets have a thickness of ~0.4 mm [127].

3. Family 1144

This new family was discovered in November 2016, where some pairs of alkali and alkaline earth elements of varying sizes lead to stoichiometric $AEAFe_4As_4$ (AE = Ca, Sr and A = K, Rb, Cs) [12] such as $CaKFe_4As_4$, $SrAFe_4As_4$ (A = Rb, Cs), $CaRbFe_4As_4$, and $CaCsFe_4As_4$. In essence, their structure is identical to the $AEFe_2As_2$ structure, just with layer by layer segregation of the AE and A ions. The reported T_c value for this 1144 family ranges from 31 to 37 K confirmed from magnetic and transport characterizations [12]. Surprisingly, these stoichiometric compounds have such a high T_c without the addition of any doping [12]. Recent studies have established that this family has a very high critical current density (J_c) of the order of 10^8 A/cm^2 and a high H_{c2} (~100 T) with very low anisotropy. Furthermore, J_c has better field dependence than the 122 family and other FBS [18]. Interestingly, high T_c values of the 1144 family are among the highest reported for bulk, fully ordered, stoichiometric FBS [12]. Hence, this family provides a wonderful opportunity to explore the superconducting properties of FBS in a highly ordered compound [17].

Furthermore, extremely high J_c and an isotropic H_{c2} of 1144 indicate significantly improved superconducting properties when compared to other FBS [18,137] families. These experimental findings recommend the 1144 family as a possible strong candidate for superconducting magnet applications where high-quality wires or tapes are required. As we know, wires and tapes for bulk applications are always based on polycrystalline materials, and we need a large quantity of high-quality polycrystalline samples [4]. Hence, an optimization of the synthesis method of 1144 powder is generally required, so that a robust synthesis process can be established for a large amount of the powder sample.

Polycrystalline: Polycrystalline 1144 samples have been synthesized by solid-state reaction (SSR) methods as similar to other FBS, as the general process of SSR is shown in Figure 2. For the first time, Iyo et al. [12] synthesized powder $CaKFe_4As_4$ by CSP-AP and found that this new 1144 phase is very sensitive to form two 122 impurity phases of $CaFe_2As_2$ and KFe_2As_2. One should keep in mind that these 122 phases are competitive during the 1144 synthesis process and are more stable than the 1144 phase. In other words, $CaFe_2As_2$ and KFe_2As_2 (122) are the two most common phases that can appear as impurity phases during the formation of $CaKFe_4As_4$. Table 1 summarizes the reported polycrystalline samples with their superconducting properties. Recently, Singh et al. [17,32] have optimized the pure phase formation of $CaKFe_4As_4$ by preparing the samples in a very broad temperature range using Ta-tube. These samples are characterized by various measurements such as XRD, magnetization, and transport to conclude. These studies find that the synthesis process of the 1144 phase has a very narrow temperature window and a small temperature difference to eliminate the impurity phases. The synthesis conditions of 955 °C for 6 h were the optimum conditions for obtaining pure polycrystalline $CaKFe_4As_4$ with the highest onset T_c value of 34.2 K, a sharp transition width of 2 K, and also a high J_c compared to other 1144 bulk samples [32]. Furthermore, the heating time dependence has also been checked with the best synthesis temperature (955 °C), which showed that samples prepared at 955 °C for a longer period (~17 h) have the tendency to start forming $CaFe_2As_2$ and KFe_2As_2 impurity phases. The field dependence of the calculated J_c for this polycrystal sample at various temperatures shows that the J_c value at 2 K is larger than 10^4 A-cm^{-2} even at 5 T and improved compared with other 1144 polycrystalline samples [32]. However, the order of such a J_c value has also been observed in polycrystalline samples of other FBS families [11,30] and it is larger than that observed in specifically processed C-doped MgB_2 [19,138].

Furthermore, Cheng et al. [139] used the Nb tube for sealing the mixture powder after it was ball milled for 10 h in an Ar atmosphere and heated the sample at 900 °C for 30 h by the CSP-AP. The final product showed some amounts of the impurity phases, such as KFe_2As_2. Recently, Masi et al. [140] carried out the mechanochemical step on precursor powder mixtures before using a solid-state reaction synthesis route (CSP-AP) to produce the $CaKFe_4As_4$ compound. This study suggests that the high-energy ball milling step could

act as a promotor for the reaction among the pure elements. This activation process of the powders significantly reduces the synthesis temperature compared to the previous literature (~900 °C). They prepared 1144 samples in the temperature range of 500–700 °C and showed that the 1144 samples prepared at 700 °C had fewer impurity phases than other samples. Masi et al. [140] also reported the effect of an alkaline or alkaline-earth depletion or an iron enrichment on the starting chemical composition: chemical variations are reflected in the formation of secondary phases without, however, significantly influencing the superconducting properties of the samples. The reported critical current density [140] is affected by extrinsic factors presented in the samples, such as pores, impurity phases, and also the observed oxygen contamination at the grain boundaries during the milling process of the powder. These studies indicate that the mechanochemically process plays an important role in reducing the synthesis temperature, which can play a significant role in the development of superconducting wires and tapes in terms of purification and densification processes. Furthermore, Ishida et al. [141] have used the Spark Plasma Sintering (SPS) techniques for the synthesis of $CaKFe_4As_4$ polycrystalline samples and the density of prepared $CaKFe_4As_4$ has been enhanced compared to conventional methods. Interestingly, the prepared 1144 phase is stable up to 500 °C during the post-annealing process. Above this temperature, the 1144 phase started to degrade into 122 phases ($CaFe_2As_2$ and KFe_2As_2). Even long-time heating such as 17 h at synthesis temperature (955 °C) also degraded the 1144 phase into 122 phases [17,32]. Hence, the reported synthesis phase diagram of 1144 has a very narrow temperature and time window for the preparation of high-quality and large amounts of samples [17,32] by the CSP-AP. A recent study based on the effects of adding low-melting-point metals (Pb, Sn, In, and Ge) to polycrystalline $CaKFe_4As_4$ (CaK1144) superconductors has also been investigated [142]. It showed that Sn addition was effective both to suppress the impurity phases as well as increase the J_c of $CaKFe_4As_4$ without affecting the T_c value, as similar to that reported for Sm1111 [106].

To understand the granular nature of the 1144 family, the remanent magnetization study based on polycrystalline [32] shows the two peaks concerning intergrain and intragrain connectivity as similar to the 1111 family [37,78]. The intergrain J_c of 1144 is shown in Figure 3, which is smaller than 122, 1111, and 11 families. This study suggests that the prepared 1144 samples are in a pure phase, but the grain connectivity is very weak due to the presence of many pores inside the sample. This means that, while pure phase formation is important for bulk superconductivity, well-grain connectivity is also required for improved superconducting properties. There is no report based on the HPST.

Single crystal: Since the stoichiometric 1144 phase has four elements, the solution growth method for the single crystal growth is challenging from a four-element melt. Furthermore, the final 1144 phase and its parent 122 phases ($AeFe_2As_2$ and AFe_2As_2) are structurally and chemically similar [12,130]. The first report based on the polycrystalline sample also suggests the similarity of the crystallographic *a*-lattice parameters between 122s is necessary for the formation of the 1144 phase [12]. Hence, during the crystallization process, 1144 phase formations are competed against by these two 122 phases, which could appear as impurities, as discussed above. The list of reported 1144 crystals is summarized in Table 2 with their growth conditions and superconducting properties. Single crystals of $CaKFe_4As_4$ are grown by high-temperature solution growth from FeAs flux at ambient pressure (FM-AP) [130,137]. As shown in Figure 4, the precursor powders were filled up and welded into a Ta-crucible, which was sealed into an evacuated silica ampoule. The growth ampoule was heated to 650 °C for 3 h and then heated to 1180 °C for 5 h. In the next step, it was cooled down to 1050 °C over 2 h, and then slowly cooled from 1050 °C to 930 °C over 30 h [130]. At the end of the reaction, the quartz tube was removed from the furnace to avoid the phase formation of the competent 122 phases. The grown $CaKFe_4As_4$ crystals are mirrorlike plates with a thickness of 100–200 μm which generally depends on the inner diameter of the crucible. Single crystals of $CaKFe_4As_4$ are not particularly air-sensitive and can remain in the air for weeks without any noticeable degradation in their appearance or physical properties [130]. Wang et al. [143] have also grown crystals

using the self-flux method (FeAs as a flux) where reaction materials were mixed and ground thoroughly in a mortar with a molar ratio of Ca: K: Fe:As = 1.1: 1: 10: 10. The average size of the grown crystals is ~1 mm. Bao et al. [135] have used RbAs as a flux to grow the millimeter-sized crystals of $RbEuFe_4As_4$ single crystals. These crystals depict the superconducting transition temperature of 36.8 K which is the highest value for the 1144 family. This report also recommends that this flux RbAs can be used to grow the single crystal of other transition metal compounds having the same crystal structure. Furthermore, single crystals of Ni-doped $CaKFe_4As_4$, i.e., $CaK(Fe_{0.949}Ni_{0.051})_4As_4$ were grown from a high-temperature Fe-As rich melt and extensively characterized using thermodynamic and transport measurements [131]. The selected crystal with dimensions of 4.0 × 4.0 × 0.1 mm^3 was used for the characterizations where the superconducting transition of 9 K and the magnetic ordering transition of ~50 K were observed for $CaK(Fe_{0.949}Ni_{0.051})_4As_4$ crystals [131]. There is not a single report based on the high-pressure growth techniques (FM-HP) [17]. We expect the high-pressure synthesis method for single crystals and polycrystalline samples will further improve the sample quality and its superconducting properties.

4. Discussion

For the 1111 family, most studies have been reported based on polycrystalline samples (Table 1) compared to single crystals (Table 2). We have plotted the transition temperature T_c and upper critical fields H_{c2} for the reported polycrystalline and single crystal 1111 samples, as shown in Figure 6. The reported high T_c of La1111, Pr1111, and Gd1111 crystals is smaller than that of their polycrystalline samples, while in the case of Sm1111 and Nd1111 crystals, the highest T_c is almost the same as that of their polycrystalline samples. The preparation of the polycrystalline sample is an easy synthesis process compared to single crystal growth. For single crystal growth, a generally high heating temperature is needed where it is a hard task to control many elements due to vaporization, such as fluorine, arsenide, potassium, etc. Initial 1111 polycrystalline samples were prepared at a high temperature such as 1200 °C and later studies show the effect of low-temperature synthesis, such as 900 °C (Table 1) where it is better to reduce the vaporization of the elements and control the composition of the final product. These effects have appeared with the improved superconducting properties of even the same composition, such as F doped Sm1111 with a high T_c of 57.8 K [29,57]. However, there is still a problem with impurity phases and the preparation of the completely pure phase formation. As a result of these factors, the reported superconducting properties contradict the sample compositions of the polycrystalline samples [11,29,34]. To overcome these problems, single crystals generally play an important role. The reported H_{c2} value is around 100 T, as shown in Figure 6, whereas the single crystals of Sm1111 show a very high H_{c2} value of over 300 T [34]. However, growing crystals of 1111 are still very challenging [50]. A few reports show the positive effects of the high-pressure techniques on growing the 1111 crystals [50], however, these crystals were limited by their compositions [50] (Table 2) and were not very suitable for many measurements due to their tiny dimensions. In the near future, we will need more devoted work in this direction through optimization of the growth parameters, flux, suitable pressure parameters, etc.

In the case of 1144, most of the work has been performed on $CaKFe_4As_4$ and $EuRbFe_4As_4$ (Tables 1 and 2). The reported T_c and H_{c2} values are depicted in Figure 7, and the reported 1144 compositions are mentioned in Tables 1 and 2. Interestingly, the highest T_c for the members of the 1144 family is the same for the polycrystalline and single-crystal samples, as depicted in Figure 7. In addition, the reported H_{c2} is around 100 T for 1144. As mentioned above, the preparation of 1144 samples, either polycrystal or single crystal, has a very narrow synthesis/growth window and the competent phase of $CaFe_2As_2$ and KFe_2As_2 during the growth. The first report of polycrystalline samples was not in a pure phase [12]. However, later studies have optimized many synthesis parameters and reported the pure phase formation of $CaKFe_4As_4$ where the grain connectivity was another issue [17,32]. In

the case of single crystals, we have to scan many crystals in the same batch of samples to find the best crystal due to the presence of competent 122 phases [130,137]. However, the average size of a crystal is around 1 mm. Recent studies have also started to work with other members of the 1144 family [133] and possible doping such as Ni at Fe sites [131].

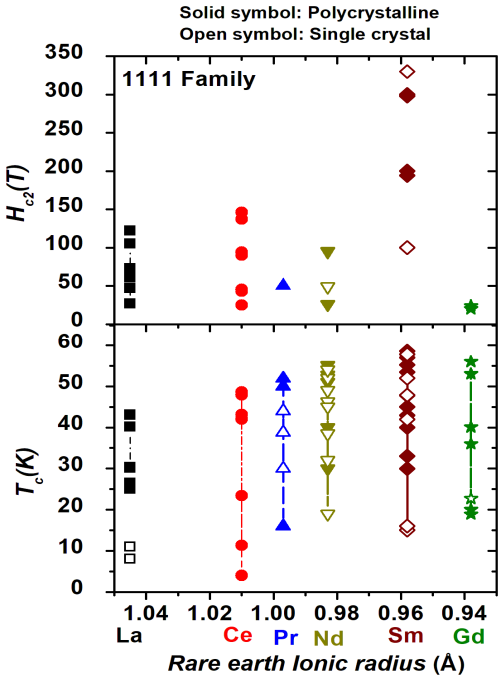

Figure 6. Upper critical field (H_{c2}) and transition temperature (T_c) values for the reported single crystal and polycrystalline 1111 (*RE*FeAsO; *RE* = rare earth) family with respect to the ionic radius of rare earth *RE* are depicted. The data have been taken from Tables 1 and 2.

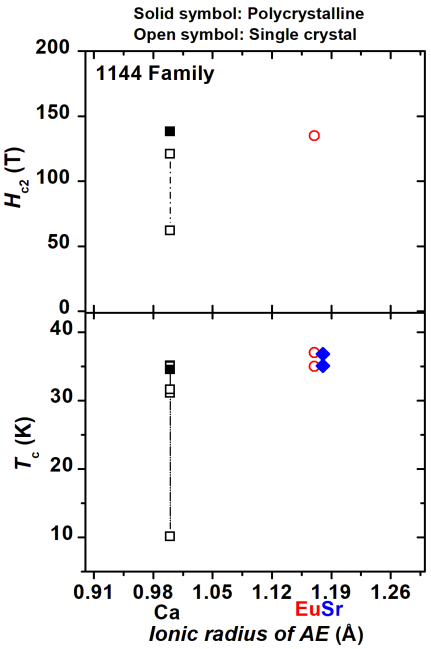

Figure 7. Upper critical field (H_{c2}) and transition temperature (T_c) values for the reported single crystal and polycrystalline 1144 ($AEAFe_4As_4$; *AE* = Ca, Eu, Sr) family with respect to the ionic radius of *AE* are shown. The data have been taken from Tables 1 and 2.

Over 10 years after the discovery of high-T_c in FBS, the synthesis processes of polycrystalline and single crystals have been improved by optimizing various growth parameters, which have enhanced their superconducting properties [18,29,32,34,106,141]. However, the low intergrain J_c value of polycrystal FBS (Figure 3) suggests the pronounced weak-link characteristics due to the presence of pores, impurity phases, and cracks at grain boundaries and sometimes even within grains. These extrinsic factors reduce the current path and transport properties of the bulk samples. Further studies will be needed to understand and reduce the effects of extrinsic factors, which will help to improve grain connectivity in the FBS polycrystalline samples. In the case of 1111 and 1144 single crystals, more studies are required to optimize the main composition and the size of a growing crystal by considering many factors such as starting composition, temperature gradient in the crucible, crucible material and size, process temperature, cooling rate, batch volume in the crucible, flux type, etc. We need to use advanced techniques such as high-energy ball milling, ultrasonic milling processes, and high-pressure techniques so that the intrinsic superconducting properties of FBS can be explored through high-quality samples. One should keep in mind that the initial synthesis process of these families is a little bit crucial due to the toxic nature of arsenic and the air sensitivity of the initial precursors. However, the prepared samples are safe and stable in the open air.

5. Conclusions

We have reviewed the growth of the single crystal and the preparation of the bulk samples of the 1111 and 1144 families with their reported superconducting properties. In the last 13 years, many synthesis parameters have been optimized by various techniques, which has led to improved sample quality and superconducting properties. Surprisingly, the highest T_c was reached in 1111 as a doped family and in 1144 as a stoichiometric compound. Additionally, in the case of the 1144 family, the J_c is extremely high, even at a high magnetic field. These unique properties require us to explore these families in more detail.

Furthermore, the 1111 family is very versatile chemically, and different types of doping have been reported in the blocking (*RE*O) and superconducting layers (FeAs), which provides an understanding of the effect of electron and hole doping. Due to the lack of high-quality and large-sized crystals, the intrinsic properties of this family have not been much explored, and the reported superconducting properties are contradictory. Interestingly, the 1144 family provides a wonderful opportunity to understand the superconducting properties of FBS in a stoichiometric compound. Based on the few studies, high-pressure growth methods are very effective for growing high-quality crystals and improving sample quality, so we need more studies in this direction for different members of these two families. Furthermore, these two families are strong contenders for practical applications, necessitating the growth of a series of high-quality single crystals and bulks to investigate the intrinsic properties of these families. This short review will be useful for the further sample growth progress of the 1111 and 1144 families, which may be beneficial for basic studies and practical applications such as superconducting wires and tapes.

Author Contributions: S.J.S. and M.I.S. have worked at the same level. All authors have read and agreed to the published version of the manuscript.

Funding: The work was supported by the National Centre for Research and Development (NCBR), Poland through Project No. POIR.04.01.02-00-0047/17 (Shiv J. Singh) and the Deutsche Forschungsgemeinschaft (DFG), Germany through Grant No. STU 695/1-1 (Mihai I. Sturza).

Acknowledgments: We would like to thank Andrzej Morawski for his support and help.

Conflicts of Interest: The authors declare no conflict of interest.

References

1. Onnes, H.K. The Superconductivity of Mercury. *Comm. Phys. Lab Uni. Leiden* **1911**, *120b*, 124c.
2. Tinkham, M. *Introduction to Superconductivity*, 2nd ed.; McGraw-Hill: New York, NY, USA, 1996; ISBN 0-486-43503-2.

3. Hosono, H.; Yamamoto, A.; Hiramatsu, H.; Ma, Y. Recent advances in iron-based superconductors toward applications. *Mater. Today* **2018**, *21*, 278–302. [CrossRef]
4. Yao, C.; Ma, Y. Recent breakthrough development in iron-based superconducting wires for practical applications. *Supercond. Sci. Technol.* **2019**, *32*, 023002. [CrossRef]
5. Johnston, D.C. The puzzle of high temperature superconductivity in layered iron pnictides and chalcogenides. *Adv. Phys.* **2010**, *59*, 803. [CrossRef]
6. Kamihara, Y.; Watanabe, T.; Hirano, M.; Hosono, H. Iron-Based Layered Superconductor La[$O_{1-x}F_x$]FeAs (x = 0.05−0.12) with Tc = 26 K. *J. Am. Chem. Soc.* **2008**, *130*, 3296. [CrossRef] [PubMed]
7. Singh, S.J.; Mele, P. Future Potential of New High Tc Iron-Based Superconductors. In *Superconductivity*; Springer: Cham, Switzerland, 2020; pp. 243–268. [CrossRef]
8. Shimoyama, J. Potentials of iron-based superconductors for practical future materials. *Supercond. Sci. Technol.* **2014**, *27*, 044002. [CrossRef]
9. Sefat, A.S.; Jin, R.; McGuire, M.A.; Sales, B.C.; Singh, D.J.; Mandrus, D. Superconductivity at 22 K in Co-Doped $BaFe_2As_2$ Crystals. *Phys. Rev. Lett.* **2008**, *101*, 117004. [CrossRef]
10. Rotter, M.; Tegel, M.; Johrendt, D. Superconductivity at 38 K in the Iron Arsenide ($Ba_{1-x}K_x$)Fe_2As_2. *Phys. Rev. Lett.* **2008**, *101*, 107006. [CrossRef]
11. Singh, S.J.; Robert, B.; Wurmehl, S.; Hess, C.; Buechner, B. Granular behavior observed in the polycrystalline superconducting LiFeAs. *Supercond. Sci. Technol.* **2015**, *28*, 025006. [CrossRef]
12. Iyo, A.; Kawashima, K.; Kinjo, T.; Nishio, T.; Ishida, S.; Fujihisa, H.; Gotoh, Y.; Kihou, K.; Eisaki, H.; Yoshida, Y. New-Structure-Type Fe-Based Superconductors: $CaAFe_4As_4$ (A = K, Rb, Cs) and $SrAFe_4As_4$ (A = Rb, Cs). *J. Am. Chem. Soc.* **2016**, *138*, 3410–3415. [CrossRef]
13. Ogino, H.; Matsumura, Y.; Katsura, Y.; Ushiyama, K.; Horii, S.; Kishio, K.; Shimoyama, J. Superconductivity at 17 K in (Fe_2P_2)($Sr_4Sc_2O_6$): A new superconducting layered pnictide oxide with a thick perovskite oxide layer. *Supercond. Sci. Technol.* **2009**, *22*, 075008. [CrossRef]
14. Zhu, X.; Han, F.; Mu, G.; Cheng, P.; Shen, B.; Zeng, B.; Wen, H.H. Transition of stoichiometric Sr_2VO_3FeAs to a superconducting state at 37.2 K. *Phys. Rev. B* **2009**, *79*, 220512. [CrossRef]
15. Ogino, H.; Shimizu, Y.; Ushiyama, K.; Kawaguchi, N.; Kishio, K.; Shimoyama, J. Superconductivity above 40 K observed in a new iron arsenide oxide (Fe_2As_2)(Ca_4(Mg,Ti)$_3O_y$). *Appl. Phys. Express* **2010**, *3*, 063103. [CrossRef]
16. Singh, S.J.; Ogino, H.; Shimoyama, J.; Kishio, K. Weak-link behaviour observed in iron-based superconductors with thick perovskite-type blocking layers. *Supercond. Sci. Technol.* **2013**, *26*, 105020. [CrossRef]
17. Singh, S.J.; Morawski, A. New Potential Family of Iron Based Superconductors towards practical application: $CaKFe_4As_4$. In *High-Tc Superconducting Technology: Towards Sustainable Development Goals*; Jenny Stanford Publishing: New York, NY, USA, 2021; pp. 283–314. [CrossRef]
18. Singh, S.J.; Bristow, M.; Meier, W.R.; Taylor, P.; Blundell, S.J.; Canfield, P.C.; Coldea, A.I. Ultrahigh critical current densities, the vortex phase diagram, and the effect of granularity of the stoichiometric high-Tc superconductor $CaKFe_4As_4$. *Phys. Rev. Mater.* **2018**, *2*, 074802. [CrossRef]
19. Buzea, C.; Yamashita, T. Review of the superconducting properties of MgB_2. *Supercond. Sci. Technol.* **2001**, *14*, R115. [CrossRef]
20. Iimura, S.; Muramoto, T.; Fujitsu, S.; Matsuishi, S.; Hosono, H. High pressure growth and electron transport properties of superconducting $SmFeAsO_{1-x}H_x$ single crystals. *J. Asian Ceram. Soc.* **2017**, *5*, 357. [CrossRef]
21. Fernandes, R.; Millies, A.J. Nematicity as a Probe of Superconducting Pairing in Iron-Based Superconductors. *Phys. Rev. Lett.* **2013**, *111*, 127001. [CrossRef]
22. Fernandes, R.M.; Chubukov, A.V.; Schmalian, J. What drives nematic order in iron-based superconductors? *Nat. Phys.* **2014**, *10*, 97. [CrossRef]
23. Chu, J.H.; Analytis, J.G.; Greve, K.; McMahon, P.L.; Islam, Z.; Yamamoto, Y.; Fisher, I.R. In-Plane Resistivity Anisotropy in an Underdoped Iron Arsenide Superconductor. *Science* **2010**, *329*, 824. [CrossRef]
24. Coldea, A. Electronic Nematic States Tuned by Isoelectronic Substitution in Bulk $FeSe_{1-x}S_x$. *Front. Phys.* **2021**, *8*, 594500. [CrossRef]
25. Wang, A.F.; Xiang, Z.J.; Ying, J.J.; Yan, Y.J.; Cheng, P.; Ye, G.J.; Luo, X.G.; Chen, X.H. Pressure effects on the superconducting properties of single-crystalline Co doped NaFeAs. *New J. Phys.* **2012**, *14*, 113043. [CrossRef]
26. Margadonna, S.; Takabayashi, Y.; Ohishi, Y.; Mizuguchi, Y.; Takano, Y.; Kagayama, T.; Nakagawa, T.; Takata, M.; Prassides, K. Pressure evolution of the low-temperature crystal structure and bonding of the superconductor FeSe. *Phys. Rev. B* **2009**, *80*, 064506. [CrossRef]
27. Sang, L.N.; Li, Z.; Yang, G.S.; Yue, Z.J.; Liu, J.X.; Cai, C.B.; Wu, T.; Dou, S.X.; Ma, Y.W.; Wang, X.L. Pressure effects on iron-based superconductor families: Superconductivity flux pinning and vortex dynamics. *Mater. Today Phys.* **2021**, *19*, 100414. [CrossRef]
28. Ge, J.F.; Liu, Z.L.; Liu, C.; Gao, C.L.; Qian, D.; Xue, Q.K.; Liu, Y.; Jia, J.F. Superconductivity above 100 K in single-layer FeSe films on doped $SrTiO_3$. *Nat. Mater.* **2015**, *14*, 285. [CrossRef]
29. Singh, S.J.; Shimoyama, J.; Yamamoto, A.; Ogino, H.; Kishio, K. Transition Temperature and Upper Critical Field in $SmFeAsO_{1-x}F_x$ Synthesized at Low Heating Temperatures. *IEEE Trans. Appl. Supercond.* **2013**, *23*, 7300605. [CrossRef]

30. Yamamoto, A.; Jiang, J.; Kametani, F.; Polyanskii, A.; Hellstrom, E.; Larbalestier, D.; Martinelli, A.; Palenzona, A.; Tropeano, M.; Putti, M. Evidence for electromagnetic granularity in polycrystalline Sm1111 iron-pnictides with enhanced phase purity. *Supercond. Sci. Technol.* **2011**, *24*, 045010. [CrossRef]
31. Kametani, F.; Polyanskii, A.A.; Yamamoto, A.; Jiang, J.; Hellstrom, E.E.; Gurevich, A.; Larbalestier, D.C.; Ren, Z.A.; Yang, J.; Dong, X.L.; et al. Combined microstructural and magneto-optical study of current flow in polycrystalline forms of Nd and Sm Fe-oxypnictides. *Supercond. Sci. Technol.* **2008**, *22*, 015010. [CrossRef]
32. Singh, S.J.; Cassidy, S.J.; Bristow, M.; Blundell, S.J.; Clarke, S.J.; Coldea, A.I. Optimization of superconducting properties of the stoichiometric $CaKFe_4As_4$. *Supercond. Sci. Technol.* **2020**, *33*, 025003. [CrossRef]
33. Iida, K.; Hanisch, J.; Yamamoto, A. Grain boundary characteristics of Fe-based superconductors. *Supercond. Sci. Technol.* **2020**, *33*, 043001. [CrossRef]
34. Fujioka, M.; Denholme, S.J.; Tanaka, M.; Takeya, H.; Yamaguchi, T.; Takano, Y. The effect of exceptionally high fluorine doping on the anisotropy of single crystalline $SmFeAsO_{1-x}F_x$. *Appl. Phys. Lett.* **2014**, *105*, 102602. [CrossRef]
35. Feldmann, D.M.; Holesinger, T.G.; Feenstra, R.; Larbalestier, D. A Review of the Influence of Grain Boundary Geometry on the Electromagnetic Properties of Polycrystalline $YBa_2Cu_3O_{7-x}$ Films. *J. Am. Ceram. Soc.* **2008**, *91*, 1869. [CrossRef]
36. Imai, Y.; Nabeshima, F.; Maeda, A. Comparative Review on Thin Film Growth of Iron-Based Superconductors. *Condens. Matter.* **2017**, *2*, 25. [CrossRef]
37. Singh, S.J.; Shimoyama, J.; Yamamoto, A.; Ogino, H.; Kishio, K. Significant enhancement of the intergrain coupling in lightly F-doped SmFeAsO superconductors. *Supercond. Sci. Technol.* **2013**, *26*, 065006. [CrossRef]
38. Ni, N.; Bud'ko, S.L.; Kreyssig, A.; Nandi, S.; Rustan, G.E.; Goldman, A.I.; Gupta, S.; Corbett, J.D.; Kracher, A.; Canfield, P.C. Anisotropic thermodynamic and transport properties of single-crystalline $Ba_{1-x}K_xFe_2As_2$ (x=0 and 0.45). *Phys. Rev. B* **2008**, *78*, 014507. [CrossRef]
39. Kihou, K.; Saito, T.; Ishida, S.; Nakajima, M.; Tomioka, Y.; Fukazawa, H.; Kohori, Y.; Ito, T.; Uchida, S.; Iyo, A.; et al. Single Crystal Growth and Characterization of the Iron-Based Superconductor KFe_2As_2 Synthesized by KAs Flux Method. *J. Phys. Soc. Jpn.* **2010**, *79*, 124713. [CrossRef]
40. Grinenko, V.; Drechsler, S.L.; Abdel-Hafiez, M.; Aswartham, S.; Wolter, A.U.B.; Wurmehl, S.; Hess, C.; Nenkov, K.; Fuchs, G.; Efremov, D.V.; et al. Disordered magnetism in superconducting KFe_2As_2 single crystals. *Phys. Status Solidi B* **2013**, *250*, 593. [CrossRef]
41. Su, M.; Link, P.; Schneidewind, A.; Wolf, T.; Adelmann, P.; Xiao, Y.; Meven, M.; Mittal, R.; Rotter, M.; Johrendt, D.; et al. Antiferromagnetic ordering and structural phase transition in $Ba_2Fe_2As_2$ with Sn incorporated from the growth flux. *Phys. Rev. B.* **2008**, *79*, 064504. [CrossRef]
42. Harnagea, L.; Singh, S.; Friemel, G.; Leps, N.; Bombor, D.; Abdel-Hafiez, M.; Wolter, A.U.B.; Hess, C.; Klingeler, R.; Behr, G.; et al. Phase diagram of the iron arsenide superconductors $Ca(Fe_{1-x}Co_x)_2As_2$ ($0 \leq x \leq 0.2$). *Phys. Rev. B* **2011**, *83*, 094523. [CrossRef]
43. Sasmal, K.; Lv, B.; Lorenz, B.; Guloy, A.M.; Chen, F.; Xue, Y.Y.; Chu, C.W. Superconducting Fe-Based Compounds $(A_{1-x}Srx)Fe_2As_2$ with A=K and Cs with Transition Temperatures up to 37 K. *Phys. Rev. Lett.* **2008**, *101*, 107007. [CrossRef]
44. Ni, N.; Nandi, S.; Kreyssig, A.; Goldman, A.I.; Mun, E.D.; Bud'ko, S.L.; Canfield, P.C. First-order structural phase transition in $CaFe_2As_2$. *Phys. Rev. B.* **2008**, *78*, 014523. [CrossRef]
45. Ni, N.; Tillman, M.E.; Yan, J.-Q.; Kracher, A.; Hannahs, S.T.; Bud'ko, S.L.; Canfield, P.C. Effects of Co substitution on thermodynamic and transport properties and anisotropic Hc_2 in $Ba(Fe_{1-x}Co_x)_2As_2$ single crystals. *Phys. Rev. B* **2008**, *78*, 214515. [CrossRef]
46. Ni, N.; Thaler, A.; Kracher, A.; Yan, J.Q.; Bud'ko, S.L.; Canfield, P.C. Phase diagrams of $Ba(Fe_{1-x}M_x)_2As_2$ single crystals (M=Rh and Pd). *Phys. Rev. B* **2009**, *80*, 024511. [CrossRef]
47. Bud'ko, S.L.; Ni, N.; Canfield, P.C. Jump in specific heat at the superconducting transition temperature in $Ba(Fe_{1-x}Co_x)_2As_2$ and $Ba(Fe_{1-x}Ni_x)_2As_2$ single crystals. *Phys Rev. B* **2009**, *79*, 220516. [CrossRef]
48. Hu, R.; Ran, S.; Straszheim, W.E.; Bud'ko, S.L.; Canfield, P.C. Single crystal growth and superconductivity of $Ca(Fe_{1-x}Co_x)_2As_2$. *Philos. Mag.* **2012**, *92*, 3113. [CrossRef]
49. Aswartham, S.; Nacke, C.; Friemel, G.; Leps, N.; Wurmehl, S.; Wizent, N.; Hess, C.; Klingeler, R.; Behr, G.; Singh, S.; et al. Single crystal growth and physical properties of superconducting ferro-pnictides $Ba(Fe, Co)_2As_2$ grown using self-flux and Bridgman techniques. *J. Cryst. Growth* **2011**, *314*, 341. [CrossRef]
50. Karpinski, J.; Zhigadlo, N.D.; Katrych, S.; Bukowski, Z.; Moll, P.; Weyeneth, S.; Keller, H.; Puzniak, R.; Tortello, M.; Daghero, D.; et al. Single crystals of $LnFeAsO_{1-x}F_x$ (Ln = La, Pr, Nd, Sm, Gd) and $Ba_{1-x}Rb_xFe_2As_2$. *Physica C* **2009**, *469*, 370. [CrossRef]
51. Bonura, M.; Giannini, E.; Viennois, R.; Senatore, C. Temperature and time scaling of the peak-effect vortex configuration in $FeTe_{0.7}Se_{0.3}$. *Phys. Rev. B* **2012**, *85*, 134532. [CrossRef]
52. Pramanik, A.K.; Harnagea, L.; Nacke, C.; Wolter, A.U.B.; Wurmehl, S.; Kataev, V.; Büchner, B. Fishtail effect and vortex dynamics in LiFeAs single crystals. *Phys. Rev. B* **2011**, *83*, 094502. [CrossRef]
53. Shen, B.; Cheng, P.; Wang, Z.; Fang, L.; Ren, C.; Shan, L.; Wen, H.H. Flux dynamics and vortex phase diagram in $Ba(Fe,Co)_2As_2$ single crystals revealed by magnetization and its relaxation. *Phys. Rev. B* **2010**, *81*, 014503. [CrossRef]
54. Prozorov, R.; Tillman, M.E.; Mun, E.D.; Canfield, P.C. Intrinsic magnetic properties of the superconductor $NdFeAsO_{0.9}F_{0.1}$ from local and global measurements. *New J. Phys.* **2009**, *11*, 035004. [CrossRef]

55. Cheng, W.; Lin, H.; Shen, B.; Wen, H.H. Comparative study of vortex dynamics in $CaKFe_4As_4$ and $Ba_{0.6}K_{0.4}Fe_2As_2$ single crystals. *Sci. Bull.* **2019**, *64*, 81. [CrossRef]
56. Wang, C.L.; Han, Q.; Wang, B.; Xie, R.; Tang, Q.; Li, Y.; Yu, B. Vortex Pinning and the Mechanism in $CaKFe_4As_4$ Revealed by Dynamical Magnetization Relaxation. *J. Supercond. Nov. Magn.* **2020**, *33*, 1979. [CrossRef]
57. Fujioka, M.; Denholme, S.J.; Ozaki, T.; Okazaki, H.; Deguchi, K.; Demura, S.; Hara, H.; Watanabe, T.; Takeya, H.; Yamaguchi, T.; et al. Phase diagram and superconductivity at 58.1 K in α-FeAs-free $SmFeAsO_{1-x}F_x$. *Supercond. Sci. Technol.* **2013**, *26*, 085023. [CrossRef]
58. Wang, X.-C.; Yu, J.; Ruan, B.B.; Pan, B.J.; Mu, Q.G.; Liu, T.; Zhao, K.; Chen, G.F.; Ren, Z.A. Revisiting the Electron-Doped SmFeAsO: Enhanced Superconductivity up to 58.6 K by Th and F Codoping. *Chin. Phys. Lett.* **2017**, *34*, 077401. [CrossRef]
59. Mu, G.; Fang, L.; Yang, H.; Zhu, X.; Cheng, P.; Wen, H.H. Doping Dependence of Superconductivity and Lattice Constants in Hole Doped $La_{1-x}Sr_xFeAsO$. *J. Phys. Soc. Jpn.* **2008**, *77*, 15. [CrossRef]
60. Ju, J.; Huynh, K.; Tang, J.; Li, Z.; Watahiki, M.; Sato, K.; Terasaki, H.; Ohtani, E.; Takizawa, H.; Tanigaki, K. Superconducting properties of $SmFeAsO_{1x}$ prepared under high-pressure condition. *J. Phys. Chem. Solids* **2010**, *71*, 491. [CrossRef]
61. Prakash, J.; Singh, S.J.; Samal, S.L.; Patnaik, S.; Ganguli, A.K. Potassium fluoride doped LaOFeAs multi-band superconductor: Evidence of extremely high upper critical field. *Europhys. Lett.* **2008**, *84*, 57003. [CrossRef]
62. Prakash, J.; Singh, S.J.; Patnaik, S.; Ganguli, A.K. Upper critical field, superconducting energy gaps and the Seebeck coefficient in $La_{0.8}Th_{0.2}FeAsO$. *J. Phys. Condens. Matter* **2009**, *21*, 175705. [CrossRef] [PubMed]
63. Prakash, J.; Singh, S.J.; Das, D.; Patnaik, S.; Ganguli, A.K. New oxypnictide superconductors: $PrOFe_{1-x}Co_xAs$. *J. Solid State Chem.* **2010**, *183*, 338. [CrossRef]
64. Prakash, J.; Singh, S.J.; Patnaik, S.; Ganguli, A.K. Superconductivity at 11.3 K induced by cobalt doping in CeFeAsO. *Solid State Commun.* **2009**, *149*, 181. [CrossRef]
65. Singh, S.J.; Shimoyama, J.; Yamamoto, A.; Ogino, H.; Kishio, K. Effects of Mn and Ni doping on the superconductivity of SmFeAs (O, F). *Phys. C Supercond.* **2013**, *494*, 57. [CrossRef]
66. Singh, S.J.; Prakash, J.; Pal, A.; Patnaik, S.; Awana, V.P.S.; Ganguli, A.K. Study of Ni and Zn doped CeOFeAs: Effect on the structural transition and specific heat capacity. *Phys. C Supercond.* **2013**, *490*, 49. [CrossRef]
67. Singh, S.J.; Shimoyama, J.; Yamamoto, A.; Ogino, H.; Kishio, K. Effects of phosphorous doping on the superconducting properties of SmFeAs (O, F). *Phys. C Supercond. Its Appl.* **2014**, *504*, 19. [CrossRef]
68. Miyazawa, K.; Kihou, K.; Ishikado, M.; Shirage, P.M.; Lee, C.H.; Takeshita, N.; Eisaki, H.; Kito, H.; Iyo, A. Synthesis of $LnFeAsO_{1-y}$ superconductors (Ln= La and Nd) using the high-pressure technique. *New J. Phys.* **2009**, *11*, 045002. [CrossRef]
69. Singh, S.J.; Prakash, J.; Patnaik, S.; Ganguli, A.K. Yttrium doped $La_{1-x}Y_xO_{0.9}F_{0.1}FeAs$ superconductors: Hall and thermopower studies. *Phys. C Supercond.* **2010**, *470*, 511. [CrossRef]
70. Tropeano, M.; Fanciulli, C.; Canepa, F.; Cimberle, M.R.; Ferdeghini, C.; Lamura, G.; Martinelli, A.; Putti, M.; Vignolo, M.; Palenzona, A. Effect of chemical pressure on spin density wave and superconductivity in undoped and 15% F-doped $La_{1-y}Y_yFeAsO$ compounds. *Phys. Rev. B* **2009**, *79*, 174523. [CrossRef]
71. Shirage, P.M.; Miyazawa, K.; Kito, H.; Eisaki, H.; Iyo, A. Superconductivity at 43 K at ambient pressure in the iron-based layered compound $La_{1-x}Y_xFeAsO_y$. *Phys. Rev. B* **2008**, *78*, 172503. [CrossRef]
72. Singh, S.J.; Prakash, J.; Patnaik, S.; Gangli, A.K. Enhancement of the superconducting transition temperature and upper critical field of $LaO_{0.8}F_{0.2}FeAs$ with antimony doping. *Supercond. Sci. Technol.* **2009**, *22*, 045017. [CrossRef]
73. Athena Sefat, S.; Huq, A.; McGuire, M.A.; Jin, R.; Sales, B.C.; Mandrus, D. Superconductivity in $LaFe_{1-x}Co_xAsO$. *Phys. Rev. B* **2008**, *78*, 104505. [CrossRef]
74. Wang, C.; Jiang, S.; Tao, Q.; Ren, Z.; Li, Y.; Li, L.; Feng, C.; Dai, J.; Cao, G.; Xu, Z. Superconductivity in $LaFeAs_{1-x}P_xO$: Effect of chemical pressures and bond covalency. *Europhys. Lett.* **2009**, *86*, 47002. [CrossRef]
75. Sato, M.; Kobayashi, Y.; Lee, S.C.; Takahashi, H.; Satomi, E.; Miura, Y. Studies of Impurity-Doping Effects and NMR Measurements of La1111 and/or Nd 1111. *J. Phys. Soc. Jpn.* **2010**, *79*, 014710. [CrossRef]
76. Miyazawa, K.; Ishida, S.; Kihou, K.; Shirage, P.M.; Nakajima, M.; Lee, C.H.; Kito, H.; Tomioka, Y.; Ito, T.; Eisaki, H.; et al. Possible hydrogen doping and enhancement of Tc in a LaFeAsO based superconductor. *Appl. Phys. Lett.* **2010**, *96*, 072514. [CrossRef]
77. Prakash, J.; Singh, S.J.; Patnaik, S.; Ganguli, A.K. Superconductivity in $CeO_{1-x}F_xFeAs$ with upper critical field of 94 T. *Phys. C Supercond.* **2009**, *469*, 82. [CrossRef]
78. Prakash, J.; Singh, S.J.; Banerjee, A.; Patnaik, S.; Ganguli, A.K. Enhancement in transition temperature and upper critical field of $CeO_{0.8}F_{0.2}FeAs$ by yttrium doping. *Appl. Phys. Lett.* **2009**, *95*, 262507. [CrossRef]
79. Luo, Y.; Li, Y.; Jiang, S.; Dai, J.; Cao, G.; Xu, Z. Phase diagram of $CeFeAs_{1-x}P_xO$ obtained from electrical resistivity, magnetization, and specific heat measurements. *Phys. Rev. B* **2010**, *81*, 134422. [CrossRef]
80. Jesche, A.; Forster, T.; Spehling, J.; Nicklas, M.; Souza, M.; Gumeniuk, R.; Luetkens, H.; Goltz, T.; Krellner, C.; Lang, M.; et al. Ferromagnetism and superconductivity in $CeFeAs_{1-x}P_xO$. *Phys. Rev. B* **2012**, *86*, 020501. [CrossRef]
81. Luo, Y.; Han, H.; Jiang, S.; Lin, X.; Li, Y.; Dai, J.; Cao, G.; Xu, Z. Interplay of superconductivity and Ce 4 f magnetism in $CeFeAs_{1-x}P_xO_{0.95}F_{0.05}$. *Phys. Rev. B* **2011**, *83*, 054501. [CrossRef]
82. Singh, S.J.; Prakash, J.; Patnaik, S.; Ganguli, A.K. Effects of simultaneous carrier doping in the charge reservoir and conducting layers of superconducting $CeO_{0.9}F_{0.1}Fe_{1-x}Co_xAs$. *Phys. C Supercond.* **2010**, *470*, 1928. [CrossRef]

83. Prakash, J.; Singh, S.J.; Thakur, G.; Patnaik, S.; Ganguli, A.K. The effect of antimony doping on the transport and magnetic properties of Ce(O/F)FeAs. *Supercond. Sci. Technol.* **2011**, *24*, 125008. [CrossRef]
84. Bhoi, D.; Mandal, P.; Choudhury, P. Normal-state transport properties of $PrFeAsO_{1-x}F_y$ superconductor. *Phys. C Supercond.* **2008**, *468*, 2275. [CrossRef]
85. Lin, X.; Guo, H.; Shen, C.; Tao, Q.; Cao, G.; Xu, Z. Superconductivity in Sr and Co co-doped PrFeAsO. *J. Phys. Chem. Solids* **2011**, *72*, 434. [CrossRef]
86. Kito, H.; Eisaki, H.; Iyo, A. Superconductivity at 54 K in F-Free $NdFeAsO_{1-y}$. *J. Phys. Soc. Jpn.* **2008**, *77*, 063707. [CrossRef]
87. Kursumovic, A.; Durrell, J.H.; Chen, S.K.; MacManus-Driscoll, J.L. Ambient/low pressure synthesis and fast densification to achieve 55 K Tc superconductivity in $NdFeAsO_{0.75}F_{0.25}$. *Supercond. Sci. Technol.* **2009**, *23*, 025022. [CrossRef]
88. Lamura, G.; Shiroka, T.; Bonfà, P.; Sanna, S.; Renzi, R.D.; Putti, M.; Zhigadlo, N.D.; Katrych, S.; Khasanov, R.; Karpinski, J. Slow magnetic fluctuations and superconductivity in fluorine-doped NdFeAsO. *Phys. Rev. B* **2015**, *91*, 024513. [CrossRef]
89. Aswathy, P.M.; Anooja, J.B.; Varghese, N.; Syamaprasad, U.U. Enhanced transport and magnetic properties in gadolinium doped $NdFeAsO_{0.7}F_{0.3}$ superconductors. *AIP Conf. Proc.* **2015**, *1665*, 130047.
90. Bérardan, D.; Zhao, L.; Pinsard-Gaudart, L.; Dragoe, N. Electronic phase diagram of $NdFe_{1-x}Rh_xAsO$. *Phys. Rev. B* **2010**, *81*, 094506. [CrossRef]
91. Lee, S.C.; Satomi, E.; Kobayashi, Y.; Sato, M. Effects of Ru Doping on the Transport Behavior and Superconducting Transition Temperature of $NdFeAsO_{0.89}F_{0.11}$. *J. Phys. Soc. Jpn.* **2010**, *79*, 023702.
92. Tehrani, F.S.; Daadmehr, V. Superconductivity Versus Structural Parameters in Calcium-Doped $Nd_{1-x}Ca_xFeAsO_{0.8}F_{0.2}$ Superconductors. *J. Supercond. Nov. Magn.* **2020**, *33*, 337. [CrossRef]
93. Marcinkova, A.; Grist, D.A.M.; Margiolaki, I.; Hansen, T.C.; Margadonna, S.; Bos, J.W. Superconductivity in $NdFe_{1-x}Co_xAsO$. *Phys. Rev. B* **2010**, *81*, 064511. [CrossRef]
94. Qi, Y.; Gao, Z.; Wang, L.; Wang, D.; Zhang, X.; Ma, Y. Superconductivity in Co-doped SmFeAsO. *Supercond. Sci. Technol.* **2008**, *21*, 115016. [CrossRef]
95. Chen, H.; Zheng, M.; Fang, A.; Yang, J.; Huang, F.; Xie, X.; Jiang, M. Enhanced superconductivity of SmFeAsO co-doped by Scandium andFluorine to increase chemical inner pressure. *J. Solid State Chem.* **2012**, *194*, 59. [CrossRef]
96. Lai, K.T.; Kwong, F.L.; Ng, D.H.L. Superconductivity in fluorine and yttrium co-doped SmFeAsO. *J. Appl. Phys.* **2012**, *111*, 093912. [CrossRef]
97. Chen, Y.L.; Cheng, C.H.; Cui, Y.J.; Zhang, H.; Zhang, Y.; Yang, Y.; Zhao, Y. Ir Doping-Induced Superconductivity in the SmFeAsO System. *J. Am. Chem. Soc.* **2009**, *131*, 10338–10339. [CrossRef] [PubMed]
98. Wang, C.; Li, L.; Chi, S.; Zhu, Z.; Ren, Z.; Li, Y.; Wang, Y.; Lin, X.; Luo, Y.; Jiang, S.; et al. Thorium-doping–induced superconductivity up to 56 K in $Gd_{1-x}Th_xFeAsO$. *Europhys. Lett.* **2008**, *83*, 67006. [CrossRef]
99. Yang, J.; Li, Z.C.; Lu, W.; Yi, W.; Shen, X.L.; Ren, Z.A.; Che, G.C.; Dong, X.L.; Sun, L.L.; Zhou, F.; et al. Superconductivity at 53.5 K in $GdFeAsO_{1-\delta}$. *Supercond. Sci. Technol.* **2008**, *21*, 082001. [CrossRef]
100. Zhou, Y.; Sidorov, V.A.; Petrova, A.E.; Penkov, A.A.; Pinyagin, A.N.; Zhao, Z.; Sun, L. Superconducting Properties of $GdFeAsO_{0.85}$ at High Pressure. *J. Supercond. Mag.* **2016**, *29*, 1105. [CrossRef]
101. Cheng, P.; Fang, L.; Yang, H.; Zhu, X.Y.; Mu, G.; Luo, H.Q.; Wang, Z.S.; Wen, H.H. Superconductivity at 36 K in gadolinium-arsenide oxides $GdO_{1-x}F_xFeAs$. *Sci. China Ser. G Phys. Mech. Astron.* **2008**, *51*, 719. [CrossRef]
102. Cui, Y.; Chen, Y.L.; Cheng, C.H.; Yang, Y.; Jiang, J.; Wang, Y.Z.; Zhang, Y.; Zhao, Y. Superconductivity and magnetism in Ir-doped GdFeAsO. *Phys. C Supercond. Its Appl.* **2010**, *470*, 1077. [CrossRef]
103. Wu, G.; Xie, Y.L.; Chen, H.; Zhong, M.; Liu, R.H.; Shi, B.C.; Li, Q.J.; Wang, X.F.; Wu, T.; Yan, Y.J. Superconductivity at 56 K in Samarium-doped SrFeAsF. *J. Phys.: Condens. Matter.* **2009**, *21*, 142203. [CrossRef]
104. Matsuishi, S.; Inoue, Y.; Nomura, T.; Yanagi, H.; Hirano, M.; Hosono, H. Superconductivity Induced by Co-Doping in Quaternary Fluoroarsenide CaFeAsF. *J. Am. Chem. Soc.* **2008**, *130*, 14428–14429. [CrossRef] [PubMed]
105. Malavasi, L.; Artioli, G.A.; Ritter, C.; Mozzati, M.C.; Maroni, B.; Pahari, B.; Caneschi, A. Phase Diagram of $NdFeAsO_{1-x}F_x$: Essential Role of Chemical Composition. *J. Am. Chem. Soc.* **2010**, *132*, 2417. [CrossRef]
106. Singh, S.J.; Shimoyama, J.; Ogino, H.; Yamamoto, A.; Kishio, K. Enhancement of intergranular current density of Sm-based oxypnictide superconductors with Sn addition. *Supercond. Sci. Technol.* **2014**, *27*, 085010. [CrossRef]
107. Otabe, E.S.; Kiuchi, M.; Kawai, S.; Morita, Y.; Ge, J.; Ni, B.; Gao, Z.; Wang, L.; Qi, Y.; Zhang, X.; et al. Global and local critical current density in superconducting $SmFeAsO_{1-x}F_x$ measured by two methods. *Phys. C Supercond.* **2009**, *469*, 1940. [CrossRef]
108. Hayashi, Y.; Yamamoto, A.; Ogino, H.; Shimoyama, J.; Kishio, K. Influences of material processing on the microstructure and inter-granular current properties of polycrystalline bulk $Ba(Fe,Co)_2As_2$. *Physica C Supercond. Its Appl.* **2014**, *504*, 28. [CrossRef]
109. Yoshida, N.; Kiuchi, M.; Otabe, E.S.; Matsushita, T.; Ge, J.; Ni, B.; Wang, L.; Qi, Y.; Zhang, X.; Gao, Z.; et al. Critical current density properties in polycrystalline $Sr_{0.6}K_{0.4}Fe_2As_2$ superconductors. *Phys. C Supercond. Its Appl.* **2010**, *470*, 1216. [CrossRef]
110. Palenzona, A.; Sala, A.; Bernini, C.; Braccini, V.; Cimberle, M.R.; Ferdeghini, C.; Lamura, G.; Martinelli, A.; Pallecchi, I.; Romano, G.; et al. A new approach for improving global critical current density in $Fe(Se_{0.5}Te_{0.5})$ polycrystalline materials. *Supercond. Sci. Technol.* **2012**, *25*, 115018. [CrossRef]
111. Quebe, P.; Terbüchte, L.J.; Jeitschko, W. Quaternary rare earth transition metal arsenide oxides RTAsO (T = Fe, Ru, Co) with ZrCuSiAs type structure. *J. Allyos Cmpds.* **2000**, *302*, 70. [CrossRef]

112. Martin, C.; Tillman, M.E.; Kim, H.; Tanatar, M.A.; Kim, S.K.; Kreyssig, A.; Gordon, R.T.; Vannette, M.D.; Nandi, S.; Kogan, V.G.; et al. Nonexponential London Penetration Depth of FeAs-Based Superconducting $ReFeAsO_{0.9}F_{0.1}$ (R = La, Nd) Single Crystals. *Phys. Rev. Lett.* **2009**, *102*, 247002. [CrossRef]
113. Fang, L.; Cheng, P.; Jia, Y.; Zhu, X.; Luo, H.; Mu, G.; Gu, C.; Wen, H.H. Growthof NdFeAs(O,F) single crystals at ambient pressure and their properties. *J. Cryst. Growth* **2009**, *311*, 358. [CrossRef]
114. Jesche, A.; Krellner, C.; Souza, M.; Lang, M.; Geibel, C. Rare earth magnetism in CeFeAsO: A single crystal study. *New J. Phys.* **2009**, *11*, 103050. [CrossRef]
115. Nitsche, F.; Jesche, A.; Hieckmann, E.; Doert, T.H.; Ruck, M. Structural trends from a consistent set of single-crystal data of RFeAsO (R = La, Ce, Pr, Nd, Sm, Gd, and Tb). *Phys. Rev. B* **2010**, *82*, 134514. [CrossRef]
116. Rutzinger, D.; Bartsch, C.; Doerr, M.; Rosner, H.; Neu, V.; Doert, T.; Ruck, M. Lattice distortions in layered type arsenides $LnTAs_2$ (Ln = La–Nd, Sm, Gd, Tb; T = Ag, Au): Crystal structures, electronic and magnetic properties. *J. Solid State Chem.* **2010**, *183*, 510. [CrossRef]
117. Hanna, A.R.N.; Abdel-Hafiez, M. Single-Crystal Growth and Small Anisotropy of the Lower Critical Field in Oxypnictides: $NdFeAsO_{1-x}F_x$. *Crystals* **2020**, *10*, 362. [CrossRef]
118. Zhigadlo, N.D.; Weyeneth, S.; Katrych, S.; Moll, P.J.W.; Rogacki, K.; Bosma, S.; Puzniak, R.; Karpinski, J.; Batlogg, B. High-pressure flux growth, structural, and superconducting properties of LnFeAsO. *Phys. Rev. B* **2012**, *86*, 214509. [CrossRef]
119. Ishida, S.; Song, D.; Ogino, H.; Iyo, A.; Eisaki, H.; Nakajima, M.; Shimoyama, J.; Eisterer, M. Doping-dependent critical current properties in K, Co, and P-doped $BaFe_2As_2$ single crystals. *Phys. Rev. B* **2017**, *95*, 014517. [CrossRef]
120. Demirdis, S.; Fasano, Y.; Kasahara, S.; Terashima, T.; Shibauchi, T.; Matsuda, Y.; Konczykowski, M.; Pastoriza, H.; Beek, C.J. Disorder, critical currents, and vortex pinning energies in isovalently substituted $BaFe_2(As_{1-x}P_x)_2$. *Phys. Rev. B* **2013**, *87*, 094506. [CrossRef]
121. Song, D.; Ishida, S.; Iyo, A.; Nakajima, M.; Shimoyama, J.; Eisterer, M.; Eisaki, H. Distinct doping dependence of critical temperature and critical current density in $Ba_{1-x}K_xFe_2As_2$ superconductor. *Sci. Rep.* **2016**, *6*, 26671. [CrossRef] [PubMed]
122. Prozorov, R.; Tanatar, M.A.; Ni, N.; Kreyssig, A.; Nandi, S.; Bud'ko, S.L.; Goldman, A.I.; Canfield, P.C. Intrinsic pinning on structural domains in underdoped single crystals of $Ba(Fe,Co)_2As_2$. *Phys. Rev. B* **2009**, *80*, 174517. [CrossRef]
123. Yan, J.Q.; Nandi, S.; Zarestky, J.L.; Tian, W.; Kreyssig, A.; Jensen, B.; Kracher, A.; Dennis, K.W.; McQueeney, R.J.; Goldman, A.I.; et al. Flux growth at ambient pressure of millimeter-sized single crystals of LaFeAsO, $LaFeAsO_{1-x}F_x$, and $LaFe_{1-x}Co_xAsO$. *Appl. Phys. Lett.* **2009**, *95*, 222504. [CrossRef]
124. Yan, J.-Q.; Jensen, B.; Dennis, K.W.; McCallum, R.W.; Lograsso, T.A. Flux requirements for the growth of RFeAsO (R = rare earth) superconductors. *Appl. Phys. Lett.* **2011**, *98*, 072504. [CrossRef]
125. Ishikado, M.; Shamoto, S.; Kito, H.; Iyo, A.; Eisaki, H.; Ito, T.; Tomioka, Y. Growth of single crystal $PrFeAsO_{1-y}$ and its characterization. *Physica C* **2009**, *469*, 901. [CrossRef]
126. Yan, J.Q.; Xing, Q.; Jensen, B.; Xu, H.; Dennis, K.W.; McCallum, R.W.; Lograsso, T.A. Contamination from magnetic starting materials in flux-grown single crystals of RFeAsO superconductors. *Phys. Rev. B* **2011**, *84*, 012501. [CrossRef]
127. Kappenberger, R.; Aswartham, S.; Scaravaggi, F.; Blum, C.; Sturza, M.I.; Wolter, A.U.B.; Wurmehl, S.; Büchner, B. Solid state single crystal growth of three-dimensional faceted LaFeAsO crystals. *J. Cryst. Growth* **2018**, *483*, 9. [CrossRef]
128. Ma, Y.; Hu, K.; Ji, Q.; Gao, B.; Zhang, H.; Mu, G.; Huang, F.; Xie, X. Growth and characterization of $CaFe_{1-x}Co_xAsF$ single crystals by CaAs flux method. *J. Cryst. Growth* **2016**, *451*, 161–164. [CrossRef]
129. Holder, M.G.; Jesche, A.; Lombardo, P.; Hayn, R.; Vyalikh, D.V.; Kummer, K.; Danzenbächer, S.; Krellner, C.; Geibel, C.; Rienks, E.D.L.; et al. How chemical pressure affects the fundamental properties of rare-earth pnictides: An ARPES view. *Phys. Rev. B* **2012**, *86*, 020506. [CrossRef]
130. Meier, W.R.; Kong, T.; Bud'ko, S.L.; Canfield, P.C. Optimization of the crystal growth of the superconductor $CaKFe_4As_4$ from solution in the FeAs-$CaFe_2As_2$-KFe_2As_2 system. *Phys. Rev. Mater.* **2017**, *1*, 013401. [CrossRef]
131. Meier, R.W.; Ding, Q.P.; Kreyssig, A.; Bud'ko, S.L.; Sapkota, A.; Kothapalli, K.; Borisov, V.; Valentí, R.; Batista, C.D.; Orth, P.P.; et al. Hedgehog spin-vortex crystal stabilized in a hole-doped iron-based superconductor. *NPJ Quantum Mater.* **2018**, *3*, 5. [CrossRef]
132. Stillwell, R.L.; Wang, X.; Wang, L.; Campbell, D.J.; Paglione, J.; Weir, S.T.; Vohra, Y.K.; Jeffries, J.R. Observation of two collapsed phases in $CaRbFe_4As_4$. *Phys. Rev. B* **2019**, *100*, 045152. [CrossRef]
133. Vlasenko, V.; Pervakov, K.; Gavrilkin, S. Vortex pinning and magnetic phase diagram of $EuRbFe_4As_4$ iron-based superconductor. *Supercond. Sci. Technol.* **2020**, *33*, 084009. [CrossRef]
134. Collomb, D.; Bending, S.J.; Koshelev, A.E.; Smylie, M.P.; Farrar, L.; Bao, J.K.; Chung, D.Y.; Kanatzidis, M.G.; Kwok, W.K.; Welp, U. Observing the Suppression of Superconductivity in $RbEuFe_4As_4$ by Correlated Magnetic Fluctuations. *Phys. Rev. Lett.* **2021**, *126*, 157001. [CrossRef] [PubMed]
135. Bao, J.K.; Willa, K.; Smylie, M.P.; Chen, H.; Welp, U.; Chung, D.Y.; Kanatzidis, M.G. Single Crystal Growth and Study of the Ferromagnetic Superconductor $RbEuFe_4As_4$. *Cryst. Growth Des.* **2018**, *18*, 3517. [CrossRef]
136. Yan, J.-Q. Flux growth utilizing the reaction between flux and crucible. *J. Cryst. Growth* **2015**, *416*, 62. [CrossRef]
137. Meier, W.R.; Kong, T.; Kaluarachchi, U.S.; Taufour, V.; Jo, N.H.; Drachuck, G.; Böhmer, A.E.; Saunders, S.M.; Sapkota, A.; Kreyssig, A.; et al. Anisotropic thermodynamic and transport properties of single-crystalline $CaKFe_4As_4$. *Phys. Rev. B* **2016**, *94*, 064501. [CrossRef]
138. Eisterer, M. Magnetic properties and critical currents of MgB_2. *Supercond. Sci. Technol.* **2007**, *20*, R47–R73. [CrossRef]

139. Cheng, Z.; Liu, S.; Dong, C.; Huang, H.; Li, L.; Zhu, Y.; Awaji, S.; Ma, Y. Effects of core density and impurities on the critical current density of $CaKFe_4As_4$ superconducting tapes. *Supercond. Sci. Technol.* **2019**, *32*, 105014. [CrossRef]
140. Masi, A.; Armenio, A.A.; Celentano, G.; Barbera, A.L.; Rufoloni, A.; Silva, E.; Vannozzi, A.; Varsano, F. The role of chemical composition in the synthesis of Ca/K-1144 iron based superconductors. *J. Alloys Compd.* **2021**, *869*, 159202. [CrossRef]
141. Ishida, S.; Naik, S.P.; Tsuchiya, Y.; Mawatari, Y.; Yoshida, Y.; Iyo, A.; Eisaki, H.; Kamiya, Y.; Kawashima, K.; Ogino, H. Synthesis of $CaKFe_4As_4$ bulk samples with high critical current density using a spark plasma sintering technique. *Supercond. Sci. Technol.* **2020**, *33*, 094005. [CrossRef]
142. Naik, S.; Ishida, S.; Kamiya, Y.; Tsuchiya, Y.; Kawashima, K.; Eisaki, H.; Iyo, A.; Ogino, H. Sn addition effects on $CaKFe_4As_4$ superconductors. *Supercond. Sci. Technol.* **2020**, *33*, 104004. [CrossRef]
143. Wang, C.; He, T.; Han, Q.; Fan, C.; Tang, Q.; Chen, D.; Lei, Q.; Sun, S.; Li, Y.; Yu, B. Novel sample-thickness-dependent flux pinning behaviors of KFe_2As_2 intercalations in $CaKFe_4As_4$ single crystals. *Supercond. Sci. Technol.* **2021**, *34*, 055001. [CrossRef]